REVIEW

Check for updates

Prospects for high-valent nickel oxides as next-generation cathodes in primary alkaline batteries

Deepika Ranganathan, [b] Yi Cai [a,b] and Madhavi Srinivasan [*a,b]

The present review casts a spotlight on the primary alkaline battery, which has humbly powered many portable electronic devices in millions of homes for more than half a century despite its non-rechargeable nature. It has remained relevant to date because of its low cost, high-energy density and environmentally safe aqueous chemistry. High-valent nickel-based oxides have emerged as a promising alternative to the conventional MnO_2 cathode owing to their higher voltage, electronic conductivity and multi-electron redox capability. Despite their considerable merits, high-valent nickel oxides suffer from rapid self-discharge and limited chemical stability in concentrated alkaline electrolytes, hindering their practical application in primary alkaline batteries. In this review, we examine high-valent nickel oxide cathodes designed for primary alkaline batteries through a nanoscale lens to unravel the critical influence of the crystalline structure of nickel oxides, cathode–electrolyte interface design and diffusion kinetics of charge carriers on electrochemical performance. A comprehensive discussion of key cathode design strategies, namely, crystal lattice engineering, bulk nanosizing, surface coating, and multiphase cathode composites, serves to illustrate how the nanoscale phenomena within the cathode can be regulated to balance discharge capacity, rate capability, and storage stability. Through systematic integration and comparison of representative high-valent nickel-based cathodes reported to date, this review bridges structural features, chemical compositions and electrochemical performance to guide the rational development of next-generation Ni–Zn primary alkaline batteries, which can fulfil the demand for high power applications.

1. Introduction

Batteries are one of the most ubiquitous and indispensable technologies in the 21st century, powering devices that range from portable electronics[1] to large-scale energy-storage devices. While rechargeable batteries dominate in electric vehicles (EVs) and grid-scale energy storage,[2] primary or non-rechargeable batteries continue to play a vital role in our everyday lives.[3] Firstly, primary batteries do not require charging before usage, rendering them useful in supporting the increasing demand for portable energy in places where connection to the main electrical grid is impossible.[4] Primary batteries are also highly suitable for low-power or low-drain consumer devices[5] commonly used in homes, such as remote controls, smoke detectors and clocks, where infrequent use and long-term storage of batteries are essential.[6] In emergency scenarios, where safety, performance and long-term reliability

supersede rechargeability, primary batteries are still critical energy sources.[7]

Several primary battery chemistries have been commercialised to date, including the zinc–carbon (Leclanché) battery, alkaline battery and lithium battery, as illustrated in Fig. 1a.[8,9] Amongst these, alkaline zinc–manganese dioxide (Zn–MnO_2) cells are most widely deployed for household electronics, capturing approximately 44% of the total primary battery market share in 2024.[10] This is attributed to the several inherent advantages of Zn–MnO_2, including its low cost, high abundance of zinc and manganese, long-term reliability, high stability over a wide temperature range and high energy density (Fig. 1c).[11] However, MnO_2 cathodes are inherently capacity-limited relative to zinc anodes, rendering the cathode as the performance-limiting component of these cells. With global demand for portable energy expected to rise steadily over the coming decade, addressing the limitations of MnO_2 cathodes has become increasingly critical.

Although manganese-based oxides have been historically designated for commercial primary alkaline batteries, their inherent bottlenecks, such as low voltage, low electronic conductivity and poor discharge capacity, compared to Ni-based oxides, have restricted their application in small electronic

[a]School of Materials Science and Engineering, Nanyang Technological University, 50 Nanyang Avenue, 639798, Singapore. E-mail: madhavi@ntu.edu.sg
[b]Energy Research Institute @ NTU (ERI@N), SCARCE Laboratory, Nanyang Technological University, 62 Nanyang Drive, Singapore 637459, Singapore
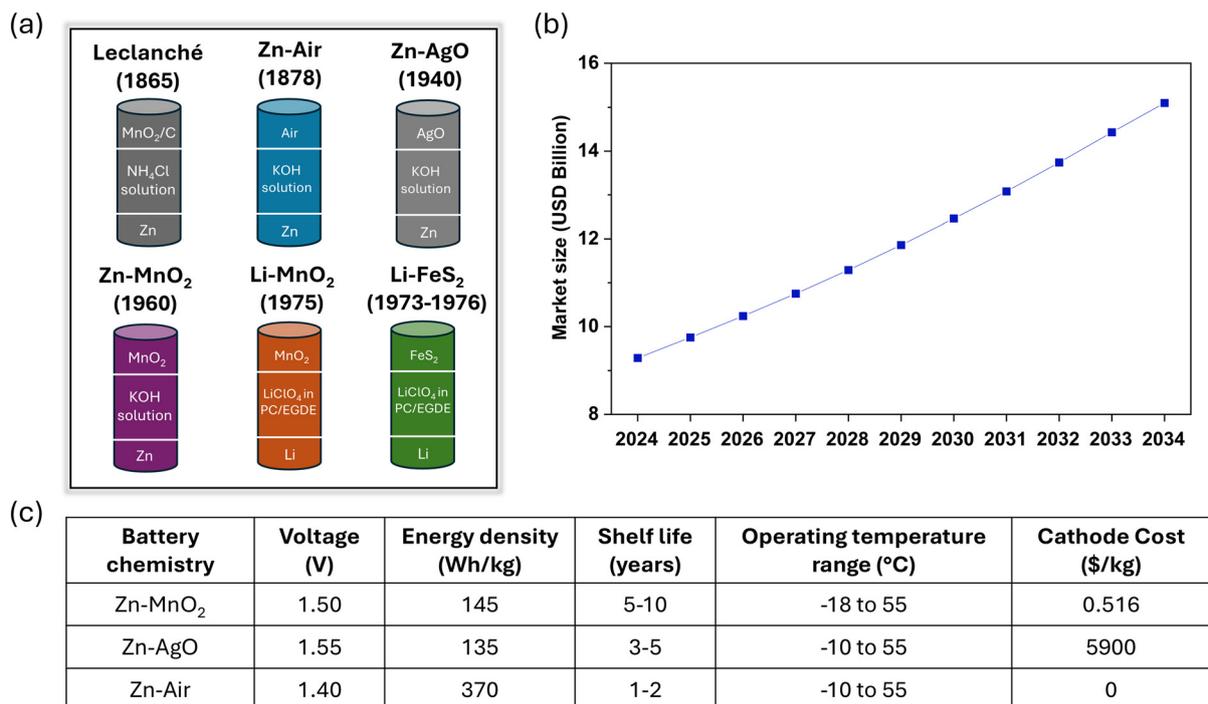
Fig. 1 (a) Overview of commercially available primary battery chemistries and the year of discovery. (b) Projected annual growth in the primary alkaline battery market size.[16] The graph was plotted based on data from ref. 16 (c) Comparative table summarizing the key features of primary alkaline batteries (Zn–MnO$_2$, Zn–AgO and Zn–air).[17–21]

Battery chemistry	Voltage (V)	Energy density (Wh/kg)	Shelf life (years)	Operating temperature range (°C)	Cathode Cost ($/kg)
Zn-MnO$_2$	1.50	145	5-10	-18 to 55	0.516
Zn-AgO	1.55	135	3-5	-10 to 55	5900
Zn-Air	1.40	370	1-2	-10 to 55	0

devices (*e.g.* remote controls, wireless computer mouse) with low power requirements. Therefore, expensive and low-abundance materials, such as lithium or silver, have been used to fulfil the current primary battery demand of critical electronic devices needing reliable and stable voltage output, which cannot be met by existing Zn–MnO$_2$ alkaline batteries. In this regard, high-valent Ni-based oxides, such as NiOOH, have emerged as promising cathode alternatives to MnO$_2$ owing to their higher conductivity, higher voltage against zinc anode, stable discharge plateau and higher theoretical capacity, which could boost their power density and energy density relative to MnO$_2$ cathodes for primary alkaline battery applications.[12–14]

Deepika Ranganathan

Deepika Ranganathan graduated with a Master of Engineering (MEng) degree in Materials Science and Engineering from Nanyang Technological University (NTU), Singapore, in 2023. Currently, she is working as a Research Associate at the Energy Research Institute at NTU (ERI@N) in Prof. Madhavi Srinivasan's group. Her research interests include investigating novel electrode architectures for energy-storage applications, such as aqueous zinc batteries and supercapacitors, as well as developing facile approaches for valuable metal recovery from waste batteries. She enjoys delving into the fundamental nanoscale mechanisms of battery materials, which are responsible for their broader electrochemical properties, to guide future synthesis optimisation studies.

Yi Cai

Yi Cai received her Ph.D. in Materials Science and Engineering from Wuhan University of Technology, China, in 2017. Since then, she has been working as a Research Fellow at Nanyang Technological University (NTU), Singapore. Her research focuses on the synthesis and engineering of nanostructured materials for energy-storage applications, including lithium-ion, aqueous zinc-ion, and alkaline batteries. Her work emphasizes structure–property–mechanism relationships in nanoscale architectures and extends to the recycling and regeneration of battery materials, aiming to bridge nanoscale materials chemistry with sustainable and circular battery technologies.

Such improvements in key performance metrics could extend the utility of future primary batteries and subsequently their lifetime before disposal.[15]

Additionally, recent advances in nanostructured Ni-based cathodes, combined with their exceptional electrochemical features, render them as attractive cathode candidates, especially with the growing incorporation of newer digital appliances with higher energy requirements in our daily lives, such as sophisticated motor-driven toys, wireless gaming controllers and portable medical devices. Although alkaline batteries perform well in commercial applications, their electrochemical performance (especially at high current densities) is still constrained by fundamental factors, such as charge-transfer kinetics, cathode–electrolyte interface stability and electronic conductivity. In Ni-based alkaline batteries, key electrochemical processes, such as proton diffusion within the layered Ni oxide framework and self-reduction at the cathode–electrolyte interface, are essentially confined to the nanoscale range. Therefore, the electrochemical behaviour of high-valent nickel cathodes cannot be fully understood and optimised solely from the perspective of bulk materials. The elucidation of the nanoscale phenomena associated with Ni cathodes, contributing to their electrochemical performance, can unlock critical insights to guide rational cathode design for primary alkaline batteries. Prominent design strategies to regulate the discharge kinetics, chemical stability and discharge capacity of Ni cathodes include particle-size reduction for shortening characteristic diffusion lengths, optimisation of interfacial stability *via* surface coatings and adjustment of cathode composition at the lattice level for interlayer stabilisation. Although several nanoscale engineering concepts were initially established for rechargeable battery chemistry, the underlying principles are directly applicable to nickel-based cathodes operating in primary alkaline batteries, where similar transport and interfacial barriers dictate their discharge performance. Therefore, well-known nanoscale engineering strategies can be reframed to address long-term trade-offs between discharge capacity, rate capability and stability of high-valent Ni cathodes in primary Ni–Zn alkaline batteries.

Since the market size for primary alkaline batteries is projected to grow steadily in the next decade, as exhibited in Fig. 1b, it is paramount that the battery chemistry can fulfil the anticipated continually rising portable energy demand, especially for high-drain applications for which Zn–MnO_2 chemistry is limited. Over the last 20 years, several advanced high-valent nickel-based cathode formulations have been reported to exhibit better performance compared to MnO_2 due to their unique nanostructural and electrochemical properties. Moreover, the surge of patents filed over the last 15 years on various novel nickel-oxide cathode formulations suggests a renewed interest of battery manufacturers in the realization of high-valent nickel oxide cathodes for primary alkaline batteries.

Owing to the considerable importance assigned to rechargeable aqueous batteries to replace or complement the toxic, flammable lithium-ion batteries for application in stationary energy-storage and small portable electronics, the majority of the review articles published on alkaline zinc batteries and Ni–Zn batteries in the last decade predominantly examine advances in Ni-based cathodes (where Ni exists as Ni^{2+}) and Zn anodes used in secondary alkaline batteries. Despite the disposable nature of primary batteries compared to their rechargeable counterparts, their numerous advantages, including zero maintenance, versatility in size, high safety, high reliability and inexpensive nature, render them relevant in this era.[17] The anticipated steadfast growth in the demand for primary alkaline batteries in the coming years justifies the present review's focus on examining the prospects of Ni-based cathodes for the next-generation of primary alkaline batteries. To date, a systematic review summarizing the structural features and electrochemical performances of nickel-based cathodes developed for primary batteries has not been reported, despite their exceptional application potential as a cathodic substitute for conventional MnO_2. As a result, substantial gaps in understanding the relationship between the crystal structure, chemical composition and electrochemical performance of nickel cathodes in primary batteries persist in current literature, which have yet to be demystified. In this review, we critically examine the current bottlenecks of the MnO_2 cathode in primary alkaline batteries, justifying the pursuit of alternative cathode materials. This is followed by a detailed introduction of the structure and electrochemistry of high-valent nickel oxides as cathode substitutes. Subsequently, various cathode engineering strategies for the development of high-valent nickel-based cathodes are discussed, providing critical insights into the optimal design of nickel oxide architecture for primary Ni–Zn alkaline batteries while uncovering the underlying nanoscale phenomena contributing to the electrochemical performance in alkaline batteries. Based on

Madhavi Srinivasan is a Professor in the School of Materials Science and Engineering at Nanyang Technological University (NTU), Singapore, and the Executive Director of the Energy Research Institute at NTU (ERI@N). Her research centres on the synthesis, fabrication, and application of nanoscale materials/architectures for electrochemical energy-storage devices, including advanced lithium-ion batteries,

Madhavi Srinivasan

aqueous zinc batteries, structural batteries and sodium-ion batteries. In addition, she serves as the Co-Director of SCARCE, a Singapore–CEA joint laboratory on circular economy and e-waste recycling, where she spearheads the development of biohydrometallurgy and direct recycling approaches for lithium-ion batteries and other types of electronic waste.

the consolidation of structural and electrochemical performance data of all high-valent nickel oxides reported in literature to date, comparative analyses of various engineered Ni oxides against commercial MnO_2 are conducted. Lastly, we conclude this review by highlighting the potential challenges in transitioning from well-known MnO_2 to nickel-based cathodes. By linking intricate design considerations of high-valent Ni cathodes and associated nanoscale phenomena with their electrochemical performance characteristics in primary alkaline batteries, this review provides guidance on the rational design of high-valent nickel-based cathodes for primary alkaline batteries of the future from a nanoscale viewpoint.

2. Redox chemistry and inherent limitations of MnO_2 cathodes

Till today, alkaline batteries continue to capture a massive share of the consumer battery market because of their high energy density and charge retention capability, which are critical performance metrics for primary batteries. MnO_2 is one of the most versatile inorganic materials, as it can exist in numerous polymorphs (α, β, γ, λ, R, δ) and present different properties.[26,27] Generally, the crystal structure of MnO_2 can be described as MnO_6 octahedra, linked to one another to form MnO_6 chains parallel to the c-axis and exhibiting specific tunnel networks,[28] which are characteristic of each polymorph, as illustrated in Fig. 2a.

As the mobility of oxygen within the MnO_2 structure, the type of OH groups present and conduciveness for proton transport are known to influence the electrochemical activity of MnO_2,[29] the selection of a suitable MnO_2 polymorph for achieving the best discharge performance is critical. Amongst all polymorphs, γ-MnO_2, which is considered a random inter-

growth of pyrolusite (β) and ramsdellite (R) phases,[30] is the most highly sought-after crystal phase for preparing alkaline battery cathodes.[31] This is attributed to the maximum availability of the tetrahedral sites of the hexagonal close-packed oxygen layers sharing zero faces with the occupied octahedral sites for proton insertion and conduction in γ-MnO_2, thus delivering the best electrochemical performance compared to other Mn polymorphs.[29,32] In fact, commercial alkaline Zn–MnO_2 cells utilize γ-MnO_2 in the form of electrolytic manganese dioxide (EMD),[33,34] which is manufactured *via* the electrodeposition of $MnSO_4$ solution in an electrolytic cell.[35] For alkaline batteries, electrochemically prepared γ-MnO_2 or EMD remains the popular choice of Mn-based cathodes because of its ease of synthesis, chemical stability at room temperature and decent electrochemical capacity. Primary Zn–MnO_2 cells are commercially available in cylindrical format (AA, AAA, C or D)[36] comprising electrolytic manganese dioxide (EMD) as the cathode active material and Zn as the anode active material.[37] The positive electrode or cathode comprises a mixture of MnO_2 powder, conductive carbon material and KOH electrolyte inserted into a steel case,[38] which serves as the current collector for the cathode. The negative electrode or anode consists primarily of Zn powder mixed with electrolyte and often a polymeric gelling agent to form a gel-based electrolyte.[36] Potassium hydroxide (KOH) is conventionally employed as the alkaline electrolyte formulation in primary alkaline cells,[25,39] owing to the high conductivity of K^+ (73.5 S cm^{-2}) compared to Li^+ (~38 S cm^{-2}) or Na^+ (~50 S cm^{-2}),[40] which improves the transportation kinetics of charge carriers responsible for the electrochemical capacity of the battery. Primary alkaline batteries generally use Zn as the anode[41] due to its favourably low reduction potential (−1.26 V *vs.* SHE) in alkaline media, which contributes to the exceptionally high voltage of alkaline bat-
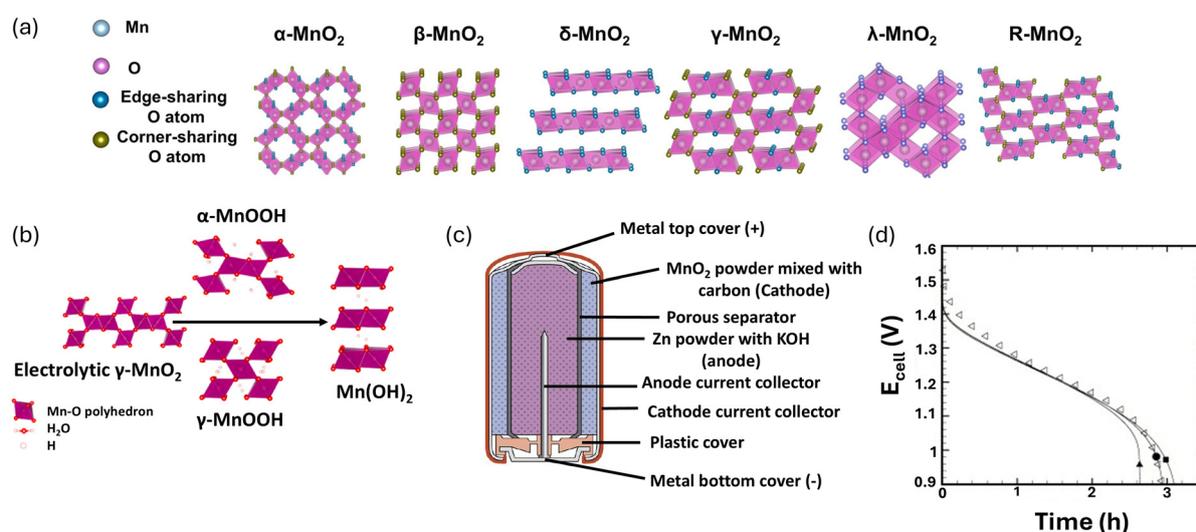
Fig. 2 (a) Various crystallographic polymorphs of MnO_2. Adapted with permission from ref. 22. Copyright 2023, Elsevier. (b) Transformation of the MnO_2 structure during the discharge process. Adapted with permission from ref. 23. Copyright 2016, the American Chemical Society. (c) Cross-section of the primary Zn–MnO_2 cell. Reproduced under the terms of the Creative Commons CC BY-NC-SA 4.0 from ref. 24. (d) Discharge curve of electrolytic manganese dioxide (EMD) in alkaline batteries. Reproduced with permission from ref. 25. Copyright 2006, Elsevier.

teries when paired with a metal oxide of Mn, Ag or Ni with a high reduction potential as the cathode material. Nevertheless, the instability and inevitable dissolution of Zn in strongly alkaline solutions limit its use to single-discharge applications in primary alkaline batteries.[42] The chemical reactions responsible for electrochemical activity in a Zn–MnO$_2$ primary alkaline battery are expressed by the cathode and anode half-reactions in Fig. 4.

Traditionally, the reaction mechanism underpinning alkaline Zn-based batteries encompasses dissolution/deposition processes at the zinc anode[43] and proton (H$^+$)-induced conversion reactions at the MnO$_2$ cathode. Therefore, the commonly proposed discharge mechanism for the MnO$_2$ cathode is the insertion of protons and electrons into the crystal structure of MnO$_2$ to form MnOOH as the predominant cathode reduction product, along with lattice enlargement.[44,45] XRD studies have confirmed that the crystal structure of the discharge product, MnOOH, resembles that of α-MnOOH.[44,46] During discharge, MnO$_2$ undergoes a one-electron reduction reaction, along with a two-electron oxidation of Zn at the anode.[47] Typically, primary alkaline batteries using MnO$_2$ cathodes are not discharged beyond the theoretical first-electron capacity of MnO$_2$ (308 mAh g^{-1}),[48] due to the unavoidable formation of resistive, electrochemically inactive products.[49] To prevent the second electron discharge of MnO$_2$ to Mn(OH)$_2$, the mass of Zn in the anode is adjusted to limit the discharge capacity of commercial cells. As shown in Fig. 2d, the discharge curve of EMD or γ-MnO$_2$ in an alkaline battery usually exhibits a characteristic slope, owing to the homogenous reduction of the MnO$_2$ cathode to form MnOOH,[50] since both the original and discharged forms of the MnO$_2$ cathode are believed to be isostructural.[44,51]

Despite the exceptional electrochemical performance, facile synthesis route, chemical stability, environmental friendliness, and low cost of the MnO$_2$ cathode for primary alkaline battery application, it is fraught with electrochemical limitations, which restrict the usage of these batteries to certain household applications. Firstly, MnO$_2$ offers a limited voltage of up to 1.6 V against zinc anodes in an alkaline system, hence limiting the overall energy density of primary Zn–MnO$_2$ batteries. Secondly, MnO$_2$ suffers from poor electronic conductivity (~10^{-5} to 10^{-6} S cm^{-1}),[52] which necessitates the addition of conductive additives, such as graphite, to improve the overall conductivity of the cathode.[53,54] Such inclusion of electrochemically inactive additives to the cathode restricts the energy density of each cell. In addition, the low electronic conductivity of MnO$_2$ results in Zn–MnO$_2$ batteries incapable of maintaining a steady voltage during discharge, making them unsuitable for high-drain devices, such as digital cameras. Thirdly, the inability to discharge beyond the first electron also limits the discharge capacity of MnO$_2$-based primary alkaline batteries. The above-mentioned drawbacks of MnO$_2$ cathode chemistry motivate the exploration of superior alternatives. Essentially, a high-energy-density battery would require three key ingredients, namely (1) a pair of cathode and anode materials exhibiting a large potential difference to provide a

high battery voltage, (2) reduced mass of inactive materials, and (3) more electrons transferred per molecule of the active compounds.[55] The current drawbacks of conventional MnO$_2$ cathodes in primary batteries offer opportunities to explore emerging nickel-based cathodes, which can increase the voltage of alkaline batteries, as well as facilitate more than one electron discharge.

3. High-valent nickel-based cathodes for primary alkaline batteries

Amongst many transition metal oxides, nickel oxides have been commonly investigated for use as a cathode in energy-storage devices, such as batteries and supercapacitors.[56–58] Specifically, nickel oxyhydroxide (NiOOH) has emerged as the most commonly investigated cathode alternative to MnO$_2$ in primary alkaline batteries, motivated by the higher redox potential and multi-electron transfer capability of Ni^{3+}/Ni^{4+} species. NiOOH exists in two polymorphs, namely β-NiOOH and γ-NiOOH, which differ in their structural order, interplanar distance and degree of hydration, and these structural variations directly influence electrochemical performance.[59] The original reaction scheme describing the electrochemical discharge of these two different phases of nickel (oxy)hydroxide was proposed by Bode *et al.* in the 1960s for rechargeable Ni-based batteries utilizing Ni(OH)$_2$ as the cathode,[60] as illustrated in Fig. 3a. Although this scheme was originally developed for secondary systems, such as Ni–Cd and Ni–MH batteries, it remains highly relevant for understanding the redox transitions of β-NiOOH and γ-NiOOH in primary alkaline batteries.

β-NiOOH exhibits a monoclinic structure (space group: $C2/m$), comprises half as many protons intercalated between the NiO$_2$ sheets of edge-sharing NiO$_6$ octahedra as β-Ni(OH)$_2$, and possesses an interplanar spacing of 4.7 Å.[59] In contrast, β-Ni(OH)$_2$ crystallizes in a cadmium iodide structure (space group: $P\bar{3}m1$), where NiO$_2$ materials are organised in well-ordered layers with H atoms in the interslab regions bonded to O in a tetrahedral environment.[61] Interestingly, β-NiOOH was discovered as not being isostructural with β-Ni(OH)$_2$, as was historically believed, due to the development of layer stacking faults upon charging or the oxidation of β-Ni(OH)$_2$.[62,63] The availability of proton vacancies in β-NiOOH enables its reduction to β-Ni(OH)$_2$ upon electrochemical discharge and results in 1 electron discharge capacity of 292 mAh g^{-1} in a primary alkaline battery.[64] To achieve a much higher discharge capacity from the Ni–Zn battery, β-NiOOH can be further oxidised chemically or electrochemically to γ-NiOOH (*e.g.* Na$_{0.33}$NiO$_2$(H$_2$O)$_{0.5}$).[65] This is attributed to the existence of Ni in a higher oxidation state of up to +3.67 in γ-NiOOH compared to β-NiOOH (+3.00), which facilitates exchange of more electrons compared to β-NiOOH during its discharge, translating to a much higher theoretical discharge capacity of up to 417 mAh g^{-1}.[66] Unlike β-NiOOH, γ-NiOOH adopts a rhombohedral structure (space group: $R\bar{3}m$), exhibits comparatively
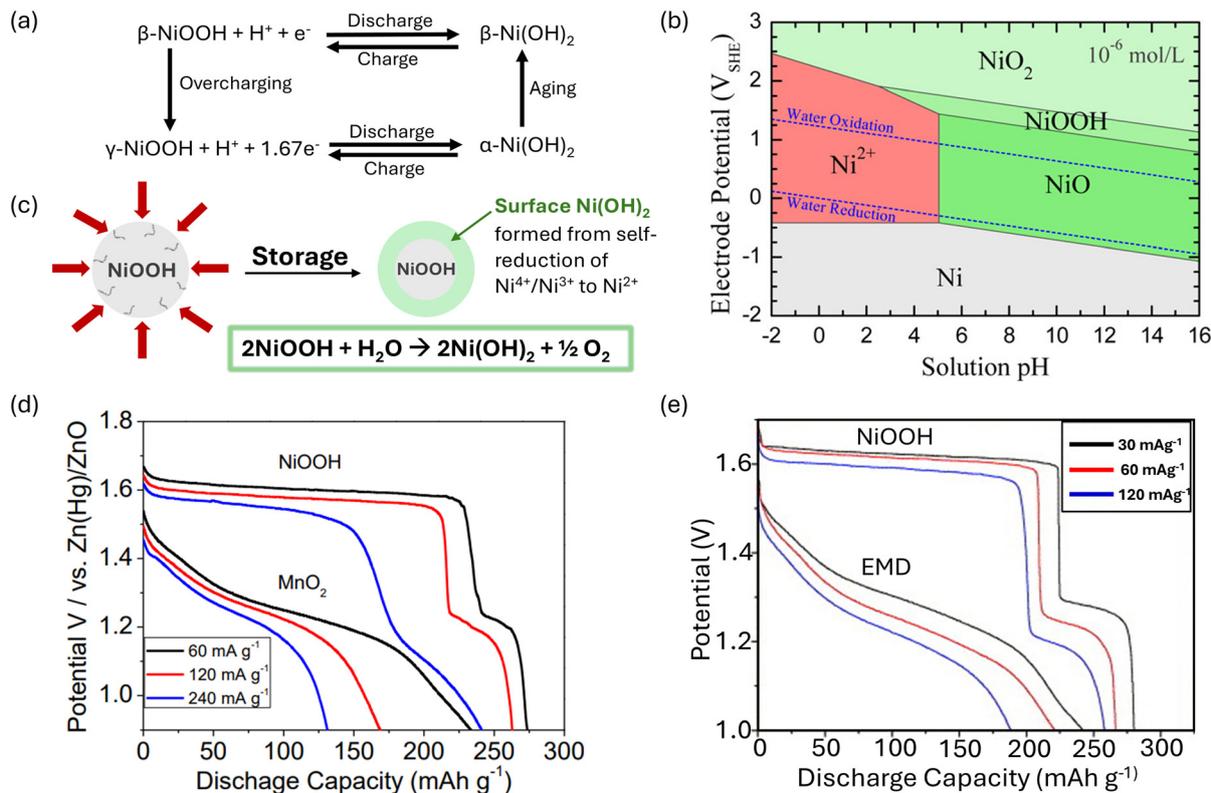
Fig. 3 (a) Overview of the reactions undergone by the Ni cathode in a rechargeable Ni–Zn alkaline battery.[60,61] (b) Nickel Pourbaix diagram. Reproduced with permission from ref. 71. Copyright 2017, the American Chemical Society. (c) Visualisation of the NiOOH cathode undergoing self-reduction to form Ni(OH)$_2$ on the surface prior to discharge under current. (d) Discharge curves of the β-NiOOH and commercial MnO$_2$ cathodes in a 6 M NaOH electrolyte at various current densities. Reproduced under the terms of the Creative Commons CC BY-NC-ND from ref. 72. Copyright 2018, Elsevier. (e) Discharge curves of NiOOH and EMD cathodes in a 9 M KOH electrolyte at various current densities. Reproduced with permission from ref. 73. Copyright 2005, Elsevier.

higher crystallinity than β-NiOOH, and accommodates Na$^+$ and/K$^+$ as well as water molecules in its interlayer spaces, which significantly increases the interslab distance to 7 Å.[67,68] As a result, γ-NiOOH can exist in a variety of chemical compositions, such as Na$_{0.33}$NiO$_2$(H$_2$O)$_{0.5}$,[69] Li$_{0.01}$Na$_{0.34}$NiO$_{1.96}$·0.5H$_2$O and Li$_{0.12}$K$_{0.21}$NiO$_{1.95}$·0.5H$_2$O.[70] As the intermediate discharged form of γ-NiOOH, α-Ni(OH)$_2$ possesses a more turbostratic structure compared to β-Ni(OH)$_2$, and hosts anions and/or water in its interlayer spaces.[61] Both β-NiOOH and γ-NiOOH are well-studied materials for primary alkaline batteries because they contain high-valent Ni (Ni^{3+} and/or Ni^{4+}) and possess layered structures with crystal vacancies suitable for proton insertion.

The electrochemical discharge of high-valent nickel oxides, such as NiOOH, has been described as the movement of the Ni(OH)$_2$/NiOOH interface from the cathode–electrolyte boundary to the cathode-current collector boundary as proton uptake occurs.[68,74] So far, thermodynamic stability predictions of H$_x$NiO$_2$ have been sparsely reported using available experimentally/theoretically determined Gibbs free energy change data.[68] First principles calculations of Gibbs free energy have demonstrated that P3 H$_x$NiO$_2$ (with AABBCC oxygen stacking sequence) is more thermodynamically stable than T1 H$_x$NiO$_2$

(with ABAB oxygen stacking sequence) when $0 < x < 1$.[75] Therefore, NiOOH inevitably undergoes stacking transformation in oxygen planes during discharge, which results in the biphasic existence of Ni(OH)$_2$ and NiOOH, as represented by the characteristically flat discharge plateau of Ni cathodes. Therefore, the length of the discharge plateau and the potential at which the plateau exists prior to the sloping discharge is often characteristic of the crystal structure of the high-valent nickel oxide phase.[75] The $R\bar{3}m$ structure is proposed to be the most energetically favourable crystal phase for γ-NiOOH (γ-H$_x$K$_{0.33}$(H$_2$O)$_{0.66}$NiO$_2$), which subsequently constrains the maximum achievable oxidation state of Ni at +3.67.[75]

To achieve higher cathode discharge capacities and voltage, tuning of the cathode crystal structure is recommended, as demonstrated in later years. Given that the proton is the charge carrier responsible for charge/discharge in Ni-based cathodes in alkaline batteries, the kinetics of the discharge process is governed by the solid-state diffusion of protons. A DFT-based study probing the favourable pathways for H$^+$ diffusion through (oxy)nickel hydroxides revealed that the interstitial addition of a proton and its transfer along the NiO$_2$ layers in the β-NiOOH phase were energetically possible, whereas travelling of H across layers along the c-axis was

impossible due to electrostatic repulsion from Ni cations.[76] Interestingly, in the past, solid-state diffusion of H^+ and OH^-/H_2O has been proposed as a dual transport mechanism within nickel (oxy)hydroxides, where interslab spacing and free/bound water play a significant role.[59,77] Such a model for charge transport within nickel cathodes supports the faster kinetics of the γ-NiOOH/α-Ni(OH)$_2$ couple with interlayer water compared to the β-NiOOH/β-Ni(OH)$_2$ couple.[59]

There are four key electrochemical advantages in adopting high-valent nickel oxides as cathode substitutes to EMD in primary alkaline batteries. Firstly, they are attractive materials for widening the overall voltage of existing alkaline batteries due to the higher reduction potential of the NiOOH/Ni(OH)$_2$ couple (+0.49 V), compared to the MnO$_2$/MnOOH couple (+0.36 V), at the cathode. This gives rise to increased voltages of the Ni–Zn battery (1.7–1.8 V) compared to the Zn–MnO$_2$ battery (1.5–1.6 V). Secondly, high-valent nickel cathodes can deliver a much higher discharge capacity compared to EMD, due to their ability to facilitate the discharge of more than 1 electron (up to 1.67 electrons for γ-NiOOH). Thirdly, the electronic conductivity of high-valent nickel oxides is much higher than that of MnO$_2$, hence requiring fewer conductive additives and enabling higher active-material utilization inside the cathode formulation to enhance the overall discharge capacity and energy density of batteries. This also translates to much higher discharge capacities at higher current rates in alkaline electrolytes compared to conventional EMD cathodes (Fig. 3d and e), rendering them suitable for high-drain electronic appli-

cations. Lastly, nickel cathodes in alkaline electrolytes provide an ultra-flat discharge plateau, characteristic of heterogeneous reaction equilibrium between discharge products and reactants, thereby providing stable voltage and reliable power output during the usage of electronic devices. Such improvements in voltage, discharge capacity and electronic conductivity would consequently improve the energy density of the Zn–NiOOH battery compared to the Zn–MnO$_2$ chemistry, as depicted in Fig. 4.

Currently, the main challenge hindering the widespread usage and commercialization of high-valent nickel oxides in primary alkaline cells is their poor stability in air and aqueous electrolytes,[78] which contributes to self-discharge of batteries.[12] As depicted by the Nickel Pourbaix diagram in Fig. 3b, nickel exists in solution as Ni^{2+} ions at lower pH values, while it exists as NiO or Ni(OH)$_2$ at higher pH values and lower potentials (vs. SHE), corresponding to the discharged state of batteries. Unfortunately, the potential window within which Ni^{2+} is oxidized to Ni^{3+} or Ni^{4+} is above the water oxidation line representing O$_2$ evolution, which is a serious issue limiting the aqueous stability of high-valent nickel cathodes. The self-reduction of NiOOH in air has also been evidenced by XPS and is postulated to occur via reaction with water in the ambient atmosphere, as illustrated in Fig. 3c.[79] The anodic partial reaction of O$_2$ evolution ($2OH^- \rightarrow \frac{1}{2}O_2 + H_2O + 2e^-$) has been experimentally confirmed as the rate-controlling step in the self-discharge of NiOOH electrodes in alkaline media.[80–83] Moreover, nickel oxyhydroxides containing proton-deficient
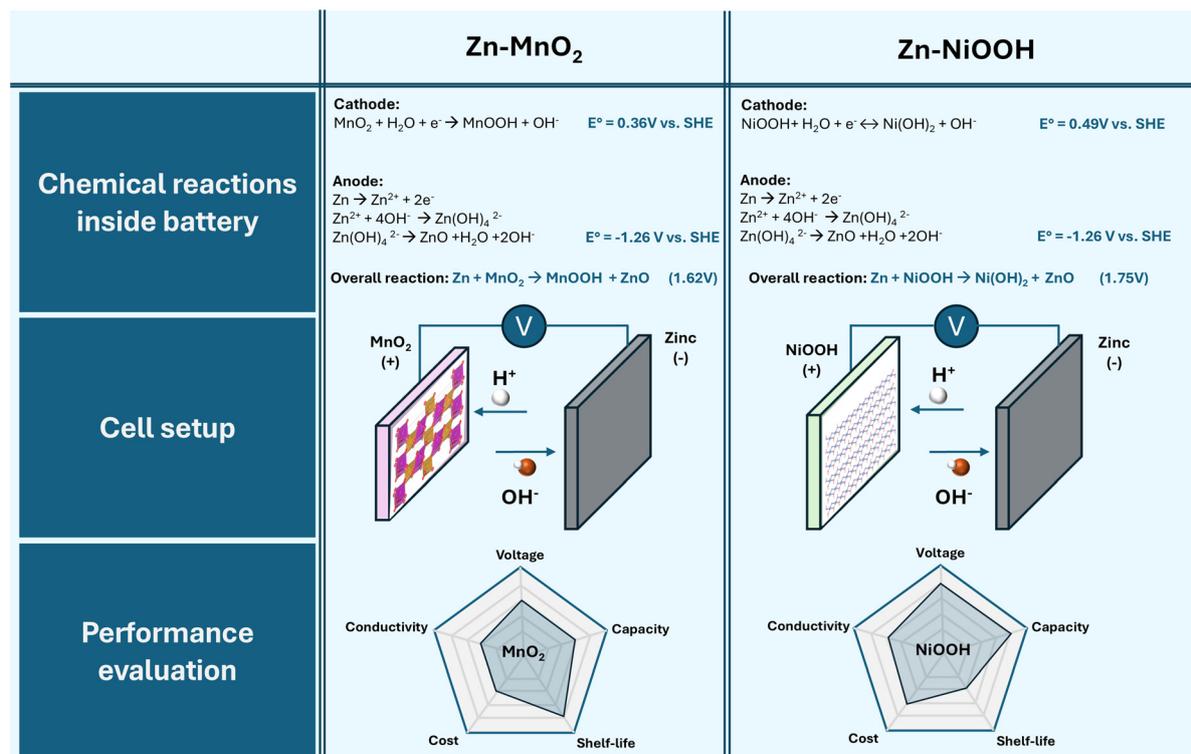

Fig. 4 Comparison of Zn–MnO$_2$ and Zn–NiOOH primary alkaline batteries based on the electrochemical reactions occurring at the cathode and anode, cell setup and performance evaluation.

surface groups have been demonstrated to be effective catalysts for the oxygen evolution reaction (OER) in alkaline media,[84] which is highly undesirable for alkaline battery application. As primary batteries are meant to be used for single-discharge applications only, it is necessary that until the battery is connected in a full circuit with the application device, the cathode remains stable and does not undergo self-discharge within the battery itself. Therefore, it is necessary to develop strategies to improve the stability of nickel cathodes in ambient air and alkaline media to fully exploit their superior electrochemical properties compared to MnO_2 for deployment in primary batteries. While several research reports on β-NiOOH and γ-NiOOH cathodes have attempted to address this prominent stability challenge for their broad application in alkaline zinc batteries,[13,85–87] as will be discussed in section 4, recent reviews have yet to consolidate and examine these design improvements in the specific context of primary alkaline batteries from a nanoscale perspective.

Ni-based cathodes ($Ni(OH)_2$) are already being used in commercial rechargeable alkaline batteries,[88,89] where metal hydride (MH) or cadmium serves as the anode active material, for powering many portable electronics.[90] However, the higher redox potential (lower oxidation potential) of these anode materials results in a lower battery voltage (~1.3 V),[91] albeit high cycling stability and specific discharge capacity of the battery, limiting the range of applications. While the Ni–Zn rechargeable alkaline battery has been actively developed by some companies,[92,93] it has yet to successfully overtake the existing Ni–MH chemistry in the market due to the inherent thermodynamic instability of Zn-based anodes in alkaline media.[18,94,95] Nevertheless, the limitations of existing MnO_2-based cathodes in alkaline batteries, as discussed previously (low electronic conductivity, voltage and specific capacity), provide considerable motivation to explore Ni-based alternatives for primary batteries for energy- and power-intensive medical devices, such as implantable defibrillators and pacemakers.[96,97]

4. Nanoscale phenomena and design strategies for high-valent Ni cathodes

Before delving into the specific material design strategies, it is necessary to first clarify the nanoscale phenomena that fundamentally determine the electrochemical behaviour of high-valent nickel cathodes. In the case of alkaline batteries, proton diffusion, surface redox and self-discharge reactions are essentially confined to the nanoscale range within the layered structure and at the cathode–electrolyte interface. Therefore, the upcoming discussion will focus on the targeted regulation of nanoscale processes *via* proposed cathode design strategies to improve the discharge performance and stability in primary alkaline batteries. Based on the well-established structural features and electrochemistry of NiOOH cathodes, two key design criteria for Ni cathodes applicable to primary alkaline batteries are derived. Firstly, the availability of crystal vacancies optimal

for proton insertion is necessary. Secondly, Ni should exist in a high valence state of +3 and/or +4 in the ideal cathode and generate $Ni(OH)_2$ upon electrochemical discharge. This would subsequently facilitate a minimum of one electron discharge in a primary battery to provide the required discharge capacity. However, the higher the valence state of nickel in the cathode, the lower its stability in the alkaline electrolyte; hence, special protection from self-reduction is required to maintain its discharge capacity close to the theoretical value. The strategic design of advanced high-valent nickel cathodes fulfilling both requirements of high shelf-life stability and discharge capacity requires an appreciation for the complex relationship between the physical, chemical, crystallographic and electrochemical properties in high-valent nickel oxides. This section uncovers suitable cathode engineering strategies and their associated nanoscale phenomena for the effective design of nickel cathodes for primary alkaline battery application by examining the cathode architecture and electrochemical performance of several high-valent nickel oxides developed to date.

Indeed, there are several approaches available for the preparation of high-valent nickel oxides (where Ni exists as Ni^{3+} or as a mixture of Ni^{3+} and Ni^{4+}), as summarized in Fig. 5. The starting precursors chosen for the synthesis would depend on the desired chemical composition and oxidation state of Ni. The higher the desired oxidation state of Ni, the higher the strength of the oxidizer required during synthesis to promote the oxidation of Ni, owing to its preferential existence as Ni^{2+} under ambient conditions.

For the successful synthesis of the pure β-NiOOH phase, the oxidation of β-$Ni(OH)_2$ using dry ozone is usually recommended to avoid intercalation of water and/or alkali metal hydrate species between NiO_2 layers.[98] Conversely, the formation of pure γ-NiOOH is achieved by the oxidation of α-$Ni(OH)_2$ or β-$Ni(OH)_2$ using potassium persulfate ($K_2S_2O_8$) or NaClO in an alkaline media to promote the insertion of alkali metal hydrate species between the NiO_2 layers *via* the expansion of the interlayer region from 0.46 nm to 0.69 nm.[12,67] Therefore, controlling the interlayer composition and crystal phase (β-NiOOH and γ-NiOOH) of the resulting nickelate derived from the $Ni(OH)_2$ precursor is only achieved by altering the choice of oxidizer and the metal substitution within the precursor itself prior to oxidation.

To further enhance the voltage and specific capacity of Ni-based cathodes beyond that achievable by conventional NiOOH cathodes, highly oxidized Ni compounds derived from layered lithium nickelate ($LiNiO_2$) and sodium nickelate ($NaNiO_2$) are promising cathode candidates.[69,99–101] Switching from proton-based nickel hydroxides to alkali metal-based nickelates as the precursor for the synthesis of high-valent Ni cathodes offers a versatile route for atomic-level tuning of the composition and interslab distance between Ni layers *via* chemical removal and retention and/or insertion of preferred interlayer species (*e.g.* Na, Li, K, H, and H_2O). Acid or oxidizer-mediated delithiation or desodiation of $LiNiO_2$ and $NaNiO_2$, respectively, can generate high-valent nickel oxides containing Ni in an oxidation state equal to or higher than that in
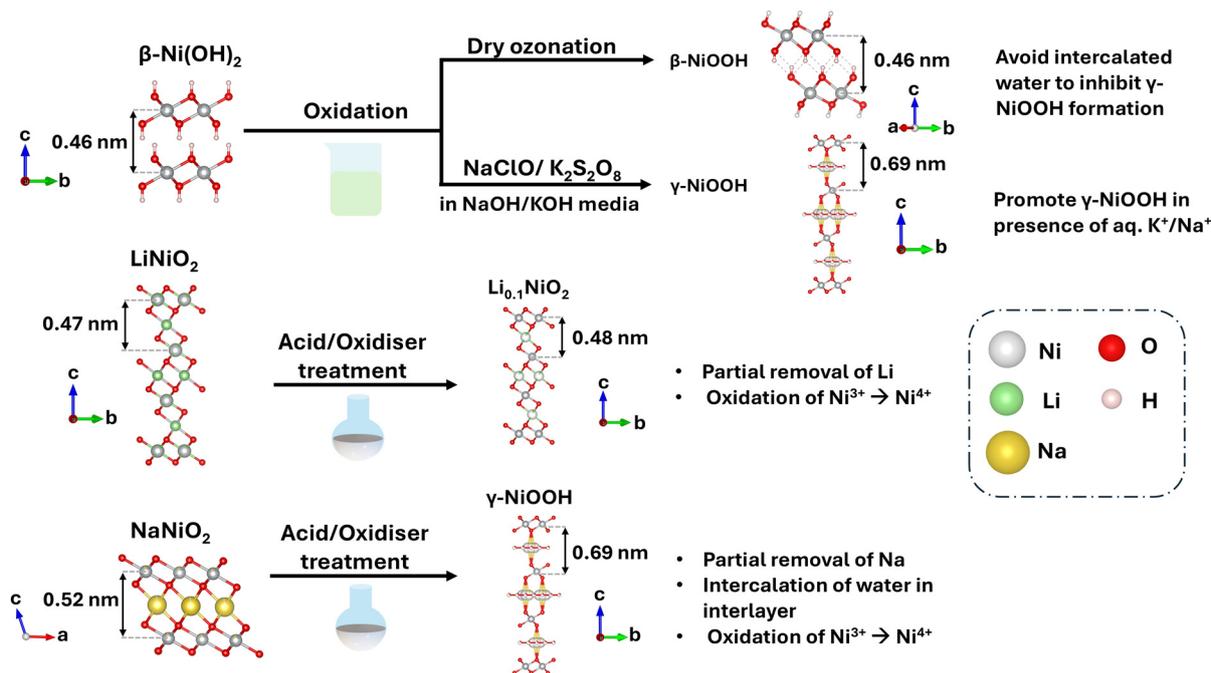
Fig. 5 Summary of basic synthesis routes adopted for the preparation of well-known high-valent nickel oxides (β-NiOOH,[62] γ-NiOOH,[69] Li$_{0.1}$NiO$_2$ [101]) using β-Ni(OH)$_2$,[102] LiNiO$_2$ [103] and NaNiO$_2$ [104] as precursors. The crystal structures of the above-mentioned compounds were visualized using the VESTA software.

β-NiOOH and comprise layered structures with metal vacancies capable of electrochemical proton uptake during discharge in an alkaline medium. The achievement of near-maximum redox of nickel would contribute to dramatic improvements in the specific capacity and energy density of the primary Ni–Zn battery. Although structural refinement studies of highly delithiated LiNiO$_2$ and desodiated NaNiO$_2$ have been reported,[69,99] none of these materials have been evaluated for application in primary alkaline batteries as the cathode active material in the literature. Instead, they have been mainly tested for application as a cathode in lithium-based cells using non-aqueous electrolyte formulations.

As emphasized earlier, due to the inherently higher redox potential and theoretical specific capacity afforded by nickel-based chemistry, high-valent nickel oxide compounds are promising cathode candidates for replacing traditional MnO$_2$ in primary alkaline batteries. It is worth noting that these advantages are not only contingent on the bulk composition but also are highly sensitive to nanoscale/atomic-level structural features, including particle size, crystal defects, surface termination, and local hydration environments. On the shortened length scale, high-valent nickel oxides exhibit significantly enhanced electrochemical activity, as well as amplified interfacial reactivity in aqueous solutions, leading to accelerated parasitic reactions and stability challenges. Meanwhile, the high material costs associated with nickel-based oxides require maximization of the utilization rate of active materials through the optimisation of the cathode architecture. Therefore, a cathode-engineering strategy that simultaneously stabilizes the redox state of high-valent nickel, regulates nanoscale interfacial reactions, and maintains high working voltage and specific capacity is imperative to overcome the commercialization obstacles of nickel-based primary alkaline cells. Based on a comprehensive examination of cathode designs and performance optimization studies reported in journal and patent literature, the following subsections unpack the key design principles and accompanying nanoscale phenomena for high-valent nickel oxide cathodes in primary alkaline batteries.

4.1. Cationic substitution/doping and nanoscale implications

Cation substitution or doping is primarily an atomic-to-lattice-scale component engineering strategy, which introduces foreign cations into the layered structure of nickel oxides to modulate charge compensation, the local coordination environment, and average interlayer spacing. Cation doping alters the crystal structure of NiO$_2$ layers and their interlayer regions, which can often be monitored through systematic changes in lattice parameters captured by X-ray diffraction (XRD) pattern refinement. Notably, atomic-level structural perturbations induced by cation doping often manifest in electrochemical implications at the nanoscale, especially in layered high-valent nickel oxides. By stabilizing the interlayer structure and proton-accessible channels, cation substitution can indirectly affect the nanoscale proton transport dynamics and interface reactivity in alkaline electrolytes. Therefore, the following discussion on cation doping/substitution regards it as a lattice-level design approach, whose broader implications on
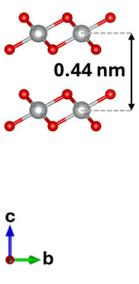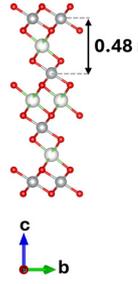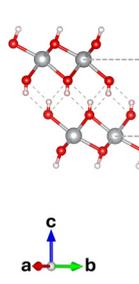
battery discharge performance can be linked to changes in nanoscale transport and interface processes at the Ni cathode. To understand the beneficial effects of doping nickel oxides on their performance as a cathode in a primary alkaline battery, the crystal structures of various layered nickel oxides of interest and their influence on electrochemistry in a primary battery will need to be discussed in depth.

In the last decade, several high-valent nickel cathode materials doped with alkali and/or transition metals have been reported to demonstrate exceptional performance for primary alkaline battery applications, affording them the present spotlight in this review for closer examination. These materials have mainly been synthesised *via* the delithiation of lithium nickelate (*e.g.*, $LiNiO_2$ and $LiNi_{1-x-y}Mn_xCo_yO_2$) or the desodia-tion of sodium nickelate ($NaNiO_2$) materials. Such high-valent nickel oxides derived from alkali metal nickelates have gained attention for primary battery applications because they contain highly oxidized nickel (Ni^{3+} and Ni^{4+}), as well as crystal vacancies suitable for protonation. Fig. 6 consolidates the crystal structures, oxidation states of Ni and theoretical specific capacities pertaining to commonly studied high-valent nickel oxides, whereas Table 1 provides a detailed breakdown of their crystal lattice parameters.

$LiNiO_2$ possesses a rhombohedral structure with trigonal symmetry (space group: $R\bar{3}m$), comprising two interpenetrating close-packed FCC sub-lattices, where one is composed of oxygen anions, and the other of Li and Ni cations on alternating (111) planes.[107,108] From a nanoscale perspective, $LiNiO_2$

Fig. 6 Crystal structures, oxidation states of Ni and theoretical specific capacities of various high-valent nickel oxides of interest in this review: NiO_2,[101] $Li_{0.1}NiO_2$[101] (a representative example of Li_xNiO_2), γ-NiOOH[69] ($Na_{0.33}NiO_2(H_2O)_{0.5}$ as a representative example) and β-NiOOH.[62] The crystal structures of the above-mentioned compounds were visualized using the VESTA software.

Table 1 Summary of the structural lattice parameters of the crystal unit cells associated with various high-valent Ni compounds

Ni compound	Chemical Treatment	Phase	*a* (nm)	*b* (nm)	*c* (nm)	*β* (°)	Phase composition (%)	Ref.
$Li_{0.1}NiO_2$	Add $LiNiO_2$ to 1.2 M sulfuric acid (25 °C, 5 h)	1	0.2818	—	1.341	—	83	100
		2	0.2815	—	1.436	—	17	
$Li_{0.04}NiO_2$	Add $LiNiO_2$ to 3.6 M sulfuric acid (25 °C, 5 h)	1	0.2821	—	1.332	—	73	99
		2	0.2818	—	1.390	—	6	
		3	0.2817	—	0.4368	—	21	
$Li_{0.47}NiO_{1.97}$	$Li_{0.1}NiO_2$ in aq. LiOH	—	0.49598	0.28283	0.50724	109.522	—	70
$Li_{0.01}Na_{0.34}NiO_{1.96}\cdot nH_2O$	$Li_{0.1}NiO_2$ in aq. NaOH	—	0.28298	—	2.0897	—	—	
$Li_{0.12}K_{0.21}NiO_{1.95}\cdot nH_2O$	$Li_{0.1}NiO_2$ in aq. KOH	—	0.28271	—	2.1090	—	—	
$Na_{0.33}NiO_2\cdot0.5H_2O$ (a form of γ-NiOOH)	Chemical oxidation of $NaNiO_2$ with Br_2	—	0.28295	—	2.09472	—	—	69
β-NiOOH	Dry ozone treatment of β-Ni(OH)$_2$	—	0.4883	0.2920	0.924	88.8	—	105

can be described as a stack of NiO_6 octahedral layers separated by alkali ion layers, where the stability of the layered framework is determined by local octahedral distortion, interslab spacing, and charge compensation at the sub-nanometer length scale. As a representative case study, Li-doped nickel oxides (Li_xNiO_2) derived from the chemical delithiation of $LiNiO_2$ exemplify how these factors determine electrochemical performance and chemical stability. At 10% Li doping in the alkali metal layer, $Li_{0.1}NiO_2$ comprises a biphasic mixture with slightly reduced unit cell dimensions (a and c), compared to pristine $LiNiO_2$ (a = 0.2875 nm, c = 1.4193 nm). When the quantity of Li dopant is reduced from 10% to 4% in $Li_{0.04}NiO_2$, a triphasic mixture exhibiting a more pronounced drop in unit cell dimensions is achieved, where the c parameter of phase 3 (comprising 21% of the resulting material) dramatically drops from 1.419 to 0.4368 nm (Table 1).[99,101] This particular phase of $Li_{0.04}NiO_2$ has been hypothesised to be hexagonal NiO_2 (space group: $P\bar{3}m1$) with a cadmium iodide structure, as evidenced by the splitting of the most intense XRD peak of Li_xNiO_2 at $2\theta = 20°$ in Fig. 7(a). The partial formation of NiO_2 implies the absence of interlayer species to balance the strong electrostatic repulsion between oxygen planes, resulting in the rearrangement of the original lithium-containing Li_xNiO_2 ($R\bar{3}m$) structure into a more thermodynamically stable assembly suitable for NiO_2 ($P\bar{3}m1$). By varying the level of Li dopant between the NiO_2 layers, the discharge capacity and chemical stability in alkaline media of the resulting high-valent nickel cathode can be tuned according to the following trend:

Theoretical discharge capacity (in $mAh\ g^{-1}$):

$$Li_{0.1}NiO_2\ (557)\ <\ Li_{0.04}NiO_2\ (577)\ <\ NiO_2\ (591)$$

Stability:

$$NiO_2\ (O.S_{Ni} = +4)\ <\ Li_{0.04}NiO_2\ (O.S_{Ni} = +3.96)$$
$$<\ Li_{0.1}NiO_2\ (O.S_{Ni} = +3.9),$$

where $O.S_{Ni}$ refers to the oxidation state of Ni.

As the quantity of Li dopant within Li_xNiO_2 decreases, the concentration of Ni^{4+} and the available crystal vacancies for protonation within the crystal framework of Ni oxide increase, contributing to its high discharge capacity and voltage when discharged immediately upon cell assembly (Fig. 7f). Despite the theoretical capacity of NiO_2 (591 $mAh\ g^{-1}$) surpassing that of $Li_{0.1}NiO_2$ (557 $mAh\ g^{-1}$), NiO_2 is considered the most unstable form of nickel oxide, where Ni exists solely as Ni^{4+}. This is attributed to the paucity of charge-balancing ions in the alkali metal layer, which fails to reduce the electrostatic
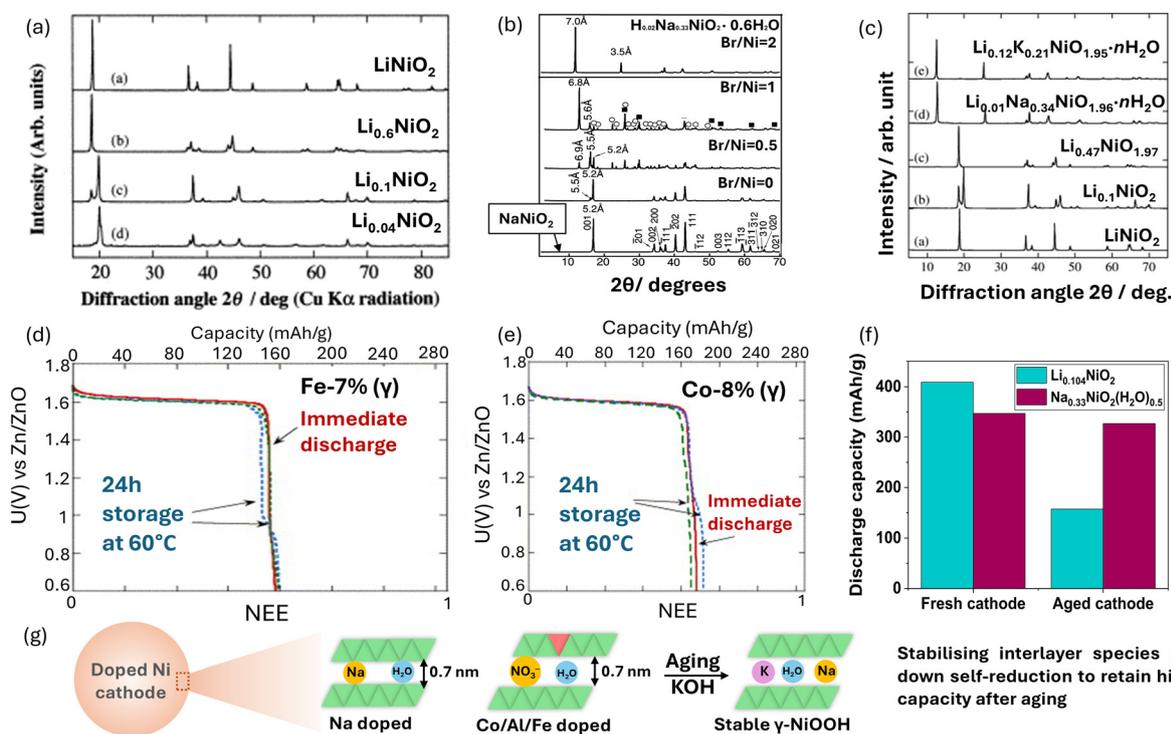
Fig. 7 Effect of cation doping/substitution on the structure and performance of nickel oxides: (a) XRD patterns of lithium nickelate with varying levels of Li doping. Adapted with permission from ref. 100. Copyright 1999, Elsevier. (b) XRD patterns of pristine $NaNiO_2$ before and after treatment in Br_2/acetonitrile solutions at different Br/Ni molar ratios ranging from 0 to 2. Adapted with permission from ref. 69. Copyright 2008, the American Chemical Society. (c) XRD patterns of nickel dioxides doped with varying amounts of alkali metals ($LiNiO_2$, $Li_{0.1}NiO_2$, $Li_{0.47}NiO_{1.97}$, $Li_{0.01}Na_{0.34}NiO_{1.96}\cdot0.5H_2O$ and $Li_{0.12}K_{0.21}NiO_{1.95}\cdot0.5H_2O$). Adapted with permission from ref. 70. Copyright 2005, Elsevier. (d) Electrochemical discharge performance of Fe-substituted γ-NiOOH and (e) co-substituted γ-NiOOH when used as the positive electrode in Ni/Zn alkaline primary button cells, where the dashed green and blue lines represent the discharge of two aged cells. Reproduced with permission from ref. 67. Copyright 2006, Elsevier. (f) Comparison of the discharge capacities of Li-doped and Na-doped nickel cathode before and after the aging test (4 weeks, 70 °C, 50% relative humidity).[106] (g) Schematic depicting the stabilisation of layered high-valent Ni cathodes after cation doping/substitution.

repulsion between O^{2-} ions in adjacent NiO_2 layers, as depicted in Fig. 6, rendering the nickel oxide highly prone to destabilisation in concentrated alkali metal hydroxide and making it an undesirable cathode candidate for long-term storage prior to discharge. Such poor chemical stability of undoped or insufficiently doped Ni cathodes (*e.g.* $Li_{0.104}NiO_2$) results in a massive drop in the discharge capacity of the cathode after aging in the electrolyte, as depicted in Fig. 7f.[106]

A direct comparison of lithium-based and sodium-based nickelates indicates that the size of the alkali ion is a powerful nano design parameter controlling the high-valent Ni oxide framework. On the contrary, chemical desodiation (by acid or other oxidising agents, such as Br_2) induces a very different structural rearrangement in $NaNiO_2$. Unlike $LiNiO_2$, $NaNiO_2$ crystallizes in the monoclinic space group ($C2/m$) at room temperature; it consists of NiO_6 octahedra, which are elongated due to the Jahn–Teller distortion of the Ni^{3+} and Na^+ ions lying between the NiO_2 slabs, and it exhibits a distorted octahedral coordination by oxygen atoms.[109,110] From a detailed examination of the XRD patterns of pristine and acid/oxidiser-treated analogues in Fig. 7a and b, it is obvious that both Li- and Na-doped nickelates, derived from the chemical oxidation of $LiNiO_2$ and $NaNiO_2$ precursors, respectively, possess very different crystal structures. From a nanoscale viewpoint, the different behaviours of $LiNiO_2$ and $NaNiO_2$ during chemical oxidation processes stem from a mismatch in length scales among the size of the alkali and nickel ions, the interlayer spacing, and the critical distances required to accommodate charge-balancing species, such as H^+ and H_2O. Since Na^+ (0.102 nm) has a larger ionic radius than Li^+ (0.074 nm), Na^+ ions pre-expand the interlayer channels compared to Li^+ ions, reducing the energy barriers for spontaneous hydration and proton insertion, thereby stabilizing the layered cathode framework.[69] Larger interlayer gaps in sodium nickelate ($d_{(001)\text{-}NaNiO_2}$ = 0.523 nm), compared to lithium nickelate ($d_{(003)\text{-}LiNiO_2}$ = 0.47 nm), may account for easier insertion of water or hydrate species between interlayer gaps, giving rise to the γ-NiOOH ($Na_{0.33}NiO_2 \cdot 0.5H_2O$) phase. Increasing the degree of oxidation of $NaNiO_2$ using a higher dosage of Br_2 led to an increased formation of the γ-NiOOH phase, as evidenced by the increasing intensity of the XRD peak corresponding to an interplanar spacing of 0.68–0.7 nm in Fig. 7b. This is attributed to the reduction in the dopant levels of Na within the nickelate structure, along with an increase in crystal-water incorporation, which favours the stabilisation of the γ-NiOOH phase.

While the complex relationship between the synthesis, structure and properties of nickel oxides has been unravelled in prior studies focused solely on $LiNiO_2$ or $NaNiO_2$, such works lack detailed comparative analyses between both materials to draw critical insights for guiding the future development of advanced nickelate cathodes for primary alkaline batteries. In the early 2000s, the partial re-insertion of Li, Na and K into delithiated lithium nickel dioxides (Li_xNiO_2) to form nickel dioxides doped with varying amounts of alkali metals, such as $Li_{0.47}NiO_{1.97}$, $Li_{0.01}Na_{0.34}NiO_{1.96} \cdot 0.5H_2O$ and

$Li_{0.12}K_{0.21}NiO_{1.95} \cdot 0.5H_2O$, has also been investigated for lithium battery applications (Fig. 7c).[70] By examining the variation in the unit cell parameters consolidated in Table 1, it was discovered that the treatment of $Li_{0.1}NiO_2$ in LiOH partially relithiates Li_xNiO_2 into $Li_{0.47}NiO_{1.97}$ by lowering the crystal symmetry from rhombohedral (space group: $R\bar{3}m$) to monoclinic (space group: $C2/m$). Increasing Li doping within nickelate from 10% to 47% improves charge shielding between adjacent oxygen planes, thereby driving nanoscale structural reorganization. In contrast, the immersion of $Li_{0.1}NiO_2$ in NaOH and KOH solutions enabled the doping of Na and K into Li_xNiO_2 to form $Li_{0.01}Na_{0.34}NiO_{1.96} \cdot 0.5H_2O$ and $Li_{0.12}K_{0.21}NiO_{1.95} \cdot 0.5H_2O$, respectively, whose crystal structures resemble the γ-NiOOH phase, as illustrated by their XRD patterns in Fig. 7c. While the *a* parameter increases imperceptibly for both resultant products, the *c* parameter increases by 0.7487 nm for the Na analogue and 0.768 nm for the K analogue while maintaining the crystal symmetry of the original structure (Table 1). The increase in the *c* parameter is indicative of water intercalation between the NiO_2 layers, along with Na^+ and K^+ ions, to stabilise the structures within the alkaline solution, which is not the case with the Li analogues.

Interestingly, it was evidenced in later works that the lower valence state of Ni in these doped nickelates (+3.5) and the presence of Na or K, along with hydrate species in their crystal structure, compared to that in the pristine delithiated Li_xNiO_2, improves the stability of the layered structure, rendering it less prone to self-reduction in an alkaline solution.[106,111] For instance, cathodes comprising high-valent nickel oxides doped with small quantities of sodium and hydrate species, identified as $Na_{0.33}NiO_2(H_2O)_{0.5}$ by XRD, discharged to a higher capacity of 327 mAh g^{-1} at a 1 V cutoff, compared to Li-doped nickel oxide ($Li_{0.104}NiO_2$) (157 mAh g^{-1}), after exposure to 70 °C/50% relative humidity for 4 weeks prior to cell discharge (Fig. 7f).[106] In summary, nanoscale tuning of the quantity and type of alkali metal doped into high-valent nickel oxides enables the achievement of decent chemical stability and high discharge capacity.

Apart from alkali metal doping, metal substitution of Ni within NiO_2 layers represents an alternative nanoscale treatment to regulate the stability of nickel oxide cathodes in primary alkaline batteries, albeit through a different mechanism. Alkali metals are doped within a metal layer separate from that of NiO_2 layers within the crystal framework of A_xNiO_2, which subsequently induces a reduction of the valence state of Ni. In contrast, doping of trivalent metal ions, such as Co^{3+} or Al^{3+}, results in the partial substitution of Ni within each NiO_2 layer of the nickelate itself, which in turn induces charge-balancing anions (*e.g.* NO_3^- and CO_3^{2-}) and hydrate species to be incorporated in the interslab region. This promotes the stabilisation of the γ-NiOOH cathode in the charged state and α-Ni(OH)$_2$ in the discharged state of the battery, as depicted in Fig. 7g. For instance, iron and cobalt substitution in the γ-NiOOH cathode was suggested to stabilise the formation of a chemically stable α-Ni(OH)$_2$ surface layer during discharge, which would subsequently slow down the

self-discharge process in a primary Ni–Zn battery to maximise the maintenance of the initial fresh cell capacity after storage at 60 °C (Fig. 7d and e).[67] The beneficial effect of such transition metal doping is further validated by early fundamental studies on nickel hydroxides and oxyhydroxides by Delmas *et al.* Their study established the stability of cobalt-substituted α-Ni(OH)$_2$ with Co content exceeding 0.2 mol% in KOH media, owing to the compensation of excess charge from trivalent Co^{3+} by the insertion of CO$_3^{2-}$ ions between NiO$_2$ layers.[112,113] The presence of charge balancing intersheet species in cobalt-substituted α-Ni(OH)$_2$ and γ-NiOOH was confirmed by the considerable increase in the *c* cell parameter of Co^{3+}-substituted α-Ni(OH)$_2$ (~0.78 nm) and Co^{3+}-substituted γ-NiOOH (~0.7 nm), relative to the Co^{3+}-substituted β-Ni(OH)$_2$ (0.46 nm).[114] Similar maintenance of large interplanar spacings after the oxidation of Al^{3+}-substituted α-Ni(OH)$_2$ (0.798 nm) to Al^{3+}-substituted γ-NiOOH (0.708 nm) has also been attributed to the presence of intercalated water and NO$_3^-$. This has contributed to improving the storage stability based on a reduction in the volume of O$_2$ gas evolved (Fig. 10a), as well as the discharge performance of the Al^{3+}-substituted γ-NiOOH cathode in 9 M KOH, compared to β-NiOOH.[115] The above examples illustrate that cation doping/ substitution between NiO$_2$ layers or within each NiO$_2$ layer is a powerful tool that can be harnessed to induce nanoscale modifications to the basic crystal structure of nickel oxide to achieve the optimal compromise between electrochemical capacity and stability of nickelate cathode for primary alkaline applications.

4.2. Nanosizing of high-valent nickel oxides

From a nanoscale perspective, the performance enhancement of nano-NiOOH cathodes stems not only from the increase in surface area but also from the emergence of diffusion-constrained electrochemical behaviour when the size of the cathode particles approaches the characteristic diffusion length of protons in NiOOH. As a popular form of bulk cathode nanostructuring, nanosizing is generally utilised to enhance the rate capability of cathodes by accelerating diffusion kinetics during battery discharge,[117,118] and it has been investigated for improving the performance of NiOOH cathodes for alkaline battery applications.

Nano-NiOOH rods with a 60–150 nm size have been prepared *via* the oxidation of spherical Ni(OH)$_2$ into NiOOH and the subsequent splitting in an NaClO–NaOH solution (Fig. 8a and b).[85] By employing a sufficiently high temperature and
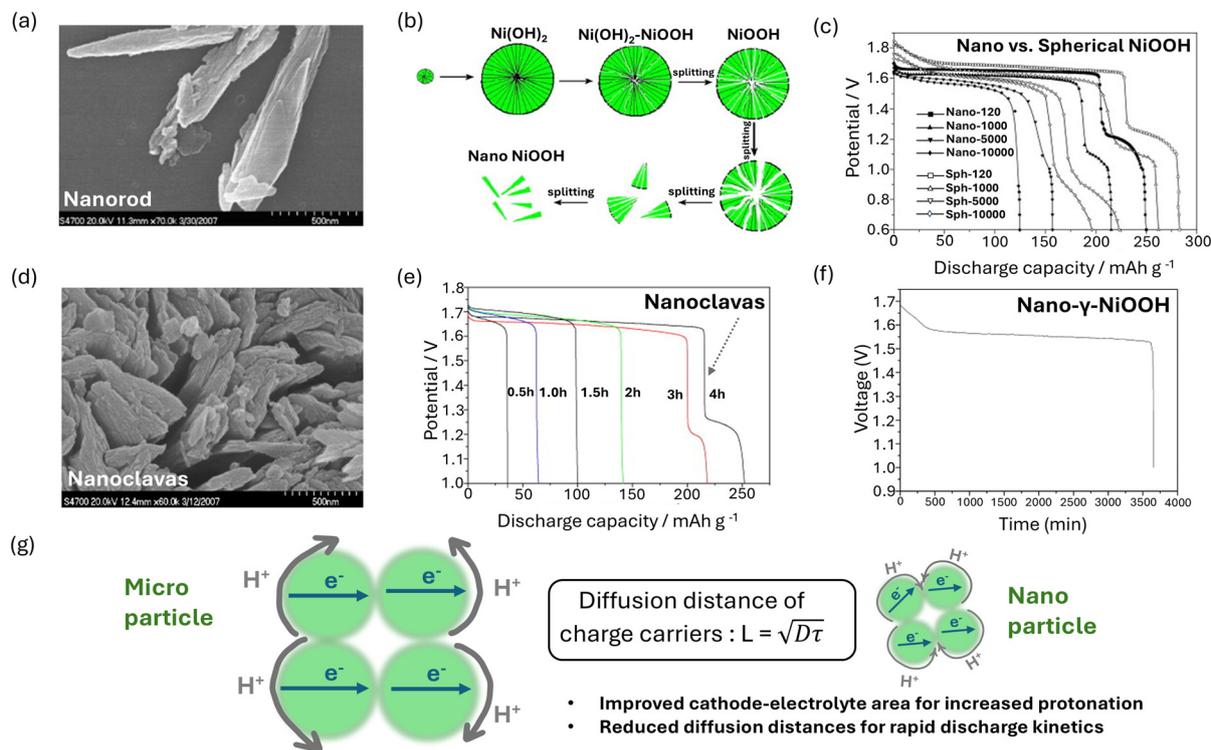
Fig. 8 (a) FESEM image of the nano-NiOOH rod prepared by 12 hours of reaction in an NaClO–NaOH solution. (b) Schematic diagram illustrating the synthesis of nano-NiOOH by the splitting method. (c) Discharge curves of the NiOOH cathodes at different discharge current densities (120 mA g^{-1}, 1000 mA g^{-1}, 5000 mA g^{-1} and 10 000 mA g^{-1}), where curves labelled 'sph' represent the performance of spherical NiOOH and 'Nano' represents that of the prepared nano-NiOOH. Adapted with permission from ref. 85. Copyright 2008, Elsevier. (d) FESEM image of the NiOOH sample obtained at the 4th hour of the oxidation process, where splitting into various nano-NiOOH clavas is observed. (e) Discharge curves of the NiOOH samples at different oxidation durations at a current density of 60 mA g^{-1}. Reproduced with permission from ref. 116 Copyright 2009, Elsevier. (f) Discharge curve of the nano γ-NiOOH cathode against a Zn anode at a constant discharge current of 5 mA. Reproduced with permission from ref. 87. Copyright 2008, Elsevier. (g) Schematic showing the change in the diffusion distances and charge-transport pathways when converting from cathode microparticles to nanoparticles.

long reaction time to facilitate the decomposition of NaClO inside the Ni(OH)$_2$ particles, the tensile force generated by oxygen evolution results in the eventual cracking or splitting of spherical NiOOH into nanorods.[116]

Using the experimentally determined value of the proton diffusion coefficient of γ-NiOOH films (4×10^{-13} cm^2 s^{-1})[119] to calculate the diffusion length (L) of protons ($L \sim \sqrt{D\tau}$, where D and τ are the diffusion coefficient and time, respectively),[120,121] it can be deduced that the discharge capacity of the cathode (when discharged in 1 minute) can be maximised by limiting the size of the γ-NiOOH cathode particles to ≤81.6 nm. This justifies the implementation of various nanosizing strategies proposed for the NiOOH cathode in a primary alkaline battery. By switching from a microspherical to nanorod morphology for the NiOOH cathode *via* the splitting method, the path lengths for both the proton and electron transport are substantially reduced, enabling high specific capacities to be achieved at high charge–discharge rates.[120] The transformation of the proton and electron transport mechanisms from the microscale to the nanoscale is reflected in the electrochemical performance in Fig. 8c, where nano-NiOOH consistently provides a higher discharge capacity over a wide range of current densities (120–10 000 mA g^{-1}).[85] It is worth noting that at high drain rates, the performance advantages become increasingly evident, highlighting the dominance of nanoscale transport limitations under actual operating conditions. Such pronounced improvement in electrochemical performance presents nano-NiOOH as a promising cathode candidate for high-drain applications requiring high discharge currents.

Detailed investigation into the synthesis process of NiOOH *via* treatment of Ni(OH)$_2$ in an NaClO–NaOH solution has revealed that prolonging the reaction time to 4 hours induces cracking of the NiOOH spheroids to form nano-NiOOH clavas (cracks within the spherical NiOOH particles) (Fig. 8d). This increases the surface area of the NiOOH cathode in contact with the electrolyte, enabling a higher discharge platform and discharge capacity when discharged at a higher current rate of 60 mA g^{-1} (Fig. 8e).[116] In another study, nano γ-NiOOH was prepared by a novel sonochemical intercalation reaction, where nickel chloride solution was added into a concentrated alkaline solution, comprising NaClO and NaOH, under low-frequency ultrasonication.[87] This method harnesses the ability of ultrasonication to facilitate insertion of alkali metal and water molecules between NiO$_2$ layers to form γ-NiOOH and simultaneously enable the dispersion of agglomerates to form nanoparticles with sizes of 1–5 nm. Under a discharge current rate of 5.65 mA g^{-1}, nano γ-NiOOH demonstrated a high discharge capacity of 350 mAh g^{-1} (Fig. 8f),[87] which approaches the theoretical discharge capacity of γ-NiOOH (417 mAh g^{-1}). This indicates that the nanoscale diffusion path limitation is the decisive factor controlling the rate performance of alkaline NiOOH cathodes. In summary, nanosizing of high-valent nickel oxides can reduce the diffusion path length of charge carriers and increase the electrode–electrolyte contact area for rate-capability enhancement of cathodes in alkaline battery (Fig. 8g). The quantitative nanoscale transport criteria provide

a reasonable basis for bulk nanosizing of Ni cathodes for high-power alkaline batteries.
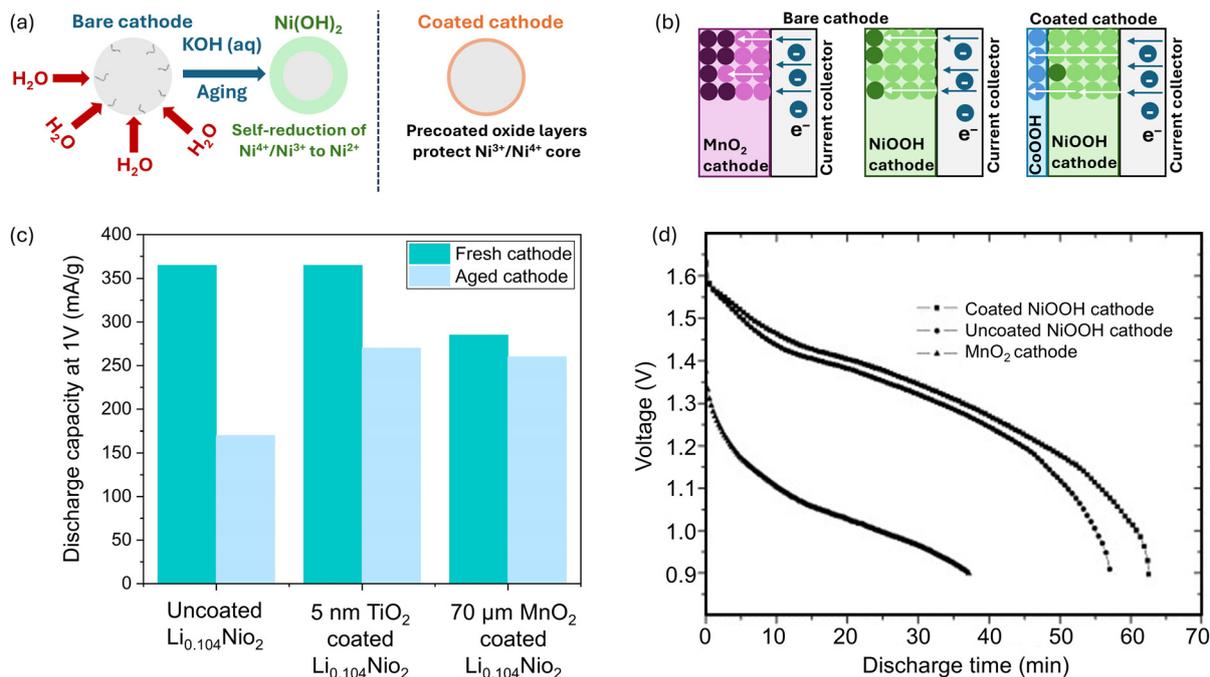
4.3. Surface coatings

The instability of high-valent nickel oxide cathodes in concentrated alkaline electrolytes originates from the interfacial self-reduction reactions that occur within the nanometer region of the cathode surface. The direct contact between highly oxidized Ni^{3+}/Ni^{4+} in the cathode surface and water molecules promotes spontaneous reduction and oxygen evolution. Therefore, in such a system, electrochemical degradation is not only controlled by bulk phase stability, but also by reaction kinetics and transport mechanisms confined to the nanoscale cathode–electrolyte interface. Surface coatings offer a method to regulate the interfacial reaction zone by introducing nanoscale barriers, selectively inhibiting parasitic chemical pathways characteristic to Ni while maintaining the electrochemical accessibility to the cathodic core material. As a form of surface nanoengineering strategy, surface coatings can be applied to the surface of cathodes to slow down or inhibit undesired reactions between the cathode particles and the external environment while maximally preserving the electrochemical activity of the cathode active material.[123] In the context of the Ni–Zn alkaline battery, the highly concentrated alkaline electrolyte (approximately 9 N or 9 M KOH) is the environment in which the surface of high-valent nickel oxide needs to be modified to improve the stability of the cathode material without sacrificing its electrochemical capacity, which is the main challenge that remains to be addressed. As highlighted earlier, high-valent Ni cathodes, such as NiOOH, can undergo self-discharge reactions during prolonged storage within concentrated KOH electrolyte, as outlined below:

$$2NiOOH + H_2O \rightarrow 2Ni(OH)_2 + \frac{1}{2}O_2$$
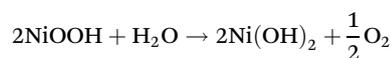
Such self-reduction or self-discharge reactions of cathodes are detrimental to the electrochemical capacity of the primary battery after prolonged storage prior to use. Since cathode discharge or self-reduction processes in alkaline media begin at the cathode–electrolyte interface and subsequently proceed inwards to the bulk of the cathode. Accordingly, the surface composition of the high-valent Ni cathode is a crucial determinant of the cathode stability. Examples of coating materials investigated for improving the stability of nickel-rich cathodes so far include carbon,[124] titanium oxide[125] and manganese oxide.[122,126] Such materials are highly attractive coating materials owing to their high inertness in concentrated alkaline solutions and the versatility of techniques available to deposit these materials as surface coatings with controlled thicknesses. As illustrated in Fig. 9a, a bare high-valent Ni cathode undergoes self-reduction commencing at the surface to form Ni(OH)$_2$ after storage in a KOH solution, while the surface coating offers protection to the inner high-valent Ni core against parasitic water activity.

For a clear visualisation of the beneficial effects of surface coatings on the cathode performance, Fig. 9c and d consoli-

Fig. 9 Influence of surface coatings on the nanoscale phenomena occurring at the cathode–electrolyte interface and the electrochemical performance of the Ni cathodes with and without surface coatings. (a) Schematic illustration of the influence of surface coating on the stability of the cathode surface region in contact with the alkaline electrolyte. (b) Schematic depiction of electron conduction and discharge reaction occurring within the MnO_2, NiOOH and coated NiOOH cathodes. (c) Bar chart of the specific discharge capacities of the uncoated, 5 nm TiO_2- and 70 μm MnO_2-coated $Li_{0.104}NiO_2$ cathodes before (fresh) and after aging tests (aged).[122] (d) Discharge curves of the Zn–NiOOH battery with and without CoOOH surface coating of the cathode as well as the Zn–MnO_2 battery as a reference. Reproduced with permission from ref. 86. Copyright 2007, Elsevier.

date the discharge performance of various nickel oxide cathodes in the presence and absence of TiO_2, MnO_2 and CoOOH surface coatings. For instance, 0.33 wt% TiO_2-coated delithiated nickelate ($Li_{0.104}NiO_2$), where the TiO_2 coating thickness is approximately 5 nm, exhibits a similar discharge capacity as the uncoated nickelate before aging tests (360–370 mAh g^{-1}) and improved capacities after 24 hours of aging (270 mAh g^{-1}) in 40 wt% KOH/6 wt% ZnO electrolyte, compared to the uncoated nickelate (170 mAh g^{-1}) (Fig. 9c).[122] Alternatively, electrochemically active and chemically stable compounds, such as MnO_2, can perform dual functions of shielding high-valent nickel from self-reduction in an electrolyte while contributing to the discharge capacity of the overall cathode when applied as a surface coating material. By exploiting the reactive and oxidative nature of pristine high-valent nickel oxides, deposition of materials *via* redox can be employed to achieve robust and intimate coatings on the nickel oxide surface. Recently, it was shown that a uniform and robust MnO_2 coating with a thickness of 70 μm, deposited by redox process on the surface of nickel oxide, results in a smaller drop in discharge capacity after prolonged aging in the electrolyte, compared to an almost 50% drop in capacity observed with the uncoated nickelate cathode (Fig. 9c).[122] While there might be a slight compromise on the capacity and voltage of the battery due to the substitution of Ni with Mn in the MnO_2-coated cathode, this is adequately compensated for

by the improved aqueous stability of the coated nickel oxide and the improvement in the electrochemical characteristics (voltage and discharge capacity), compared to the uncoated nickel oxide. Notably, the discharge capacity of the fresh TiO_2-coated nickel oxide (360–370 mAh g^{-1}) is higher than that of the MnO_2-coated nickel oxide (300 mAh g^{-1}). This is attributed to the nanometer thickness of the former coating compared to the micrometer thickness of the latter, which translates to a greater amount of active nickel oxide per unit mass of TiO_2-coated cathode.[122] Maintaining an optimal surface coating thickness of the cathode to serve as a robust passivation layer while allowing the maximum electrochemically active Ni to occupy the cathode core is imperative for achieving outstanding discharge capacity and decent stability.

The above comparison in coating thickness illustrates that the optimisation of the coating process at the nanoscale region of the cathode–electrolyte interface is critical to achieve a correct balance between chemical stability and discharge capacity of Ni-based cathodes for primary battery applications. In another instance, the application of a highly conductive thin coating of β-CoOOH (5 wt%, as determined by ICP-AES) on β-NiOOH particles improved the storage stability of the β-NiOOH cathode in 9 M KOH electrolyte, based on a reduction in the volume of O_2 gas generated (Fig. 10b), while enabling a slightly higher discharge capacity than that for an uncoated β-NiOOH cathode at a high current rate of 1A in an
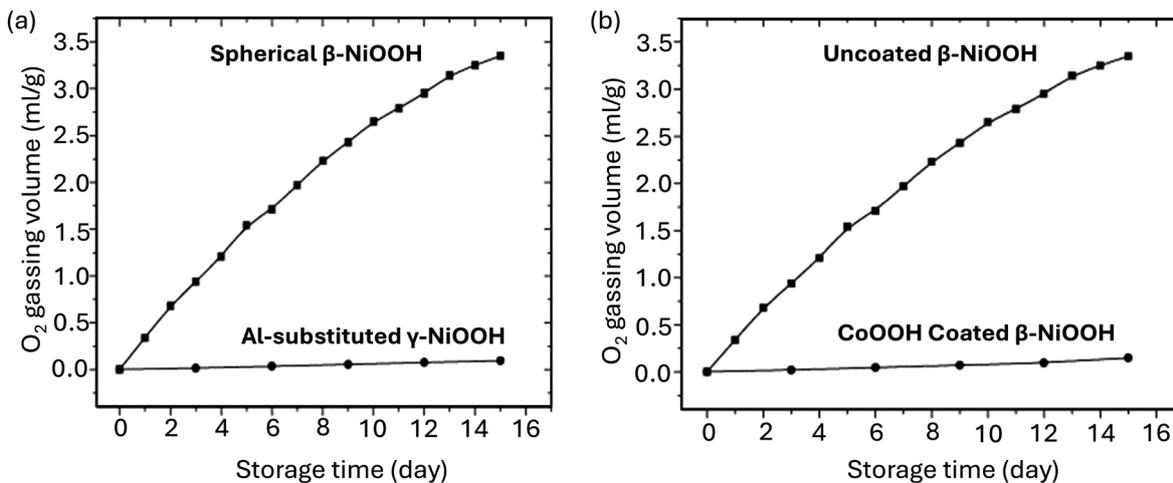
Fig. 10 O_2 evolution analyses of high-valent Ni cathodes after storage in a 9 M KOH solution at 60 °C, as a measure of the storage stability. (a) O_2 evolution measurement of the Al-substituted γ-NiOOH cathode. Reproduced with permission from ref. 115. Copyright 2007, Elsevier. (b) O_2 evolution measurement of the CoOOH-coated β-NiOOH cathodes. Reproduced with permission from ref. 86. Copyright 2007, Elsevier.

AA primary alkaline battery (Fig. 9d).[86] The outstanding electrochemical performance of the β-CoOOH-coated NiOOH cathode compared to its uncoated counterpart could be attributed to the impressive electronic conductivity of CoOOH (10^{-2} S cm^{-1})[127] and the high stability of CoOOH in alkaline media.[128] As a result, the CoOOH surface coating promotes electronic conduction, improves cathode utilisation and inhibits self-reduction within the NiOOH cathode simultaneously, relative to the bare NiOOH and MnO_2 cathodes (Fig. 9b). In a nutshell, multifunctional surface coatings possessing desirable characteristics, such as high aqueous stability, electrochemical activity and conductivity, can transform a conventionally unstable high-valent nickel oxide into an advanced cathode capable of both exceptional discharge performance

and decent chemical stability. To date, only limited studies have been conducted on the surface nanoengineering of high-valent nickel oxides for primary battery applications. Nevertheless, the exceptional electrochemical performances of surface-coated high-valent nickel cathodes reported to date serve as an important basis for future research and optimisation of surface coatings to improve the stability and discharge performance of nickel cathodes for primary alkaline batteries.

4.4. Multiphase/composite cathodes

Multi-phase cathodes or composite cathodes combine the nanoscale advantages of two or more electrochemically active cathode materials to achieve optimal discharge capacity and
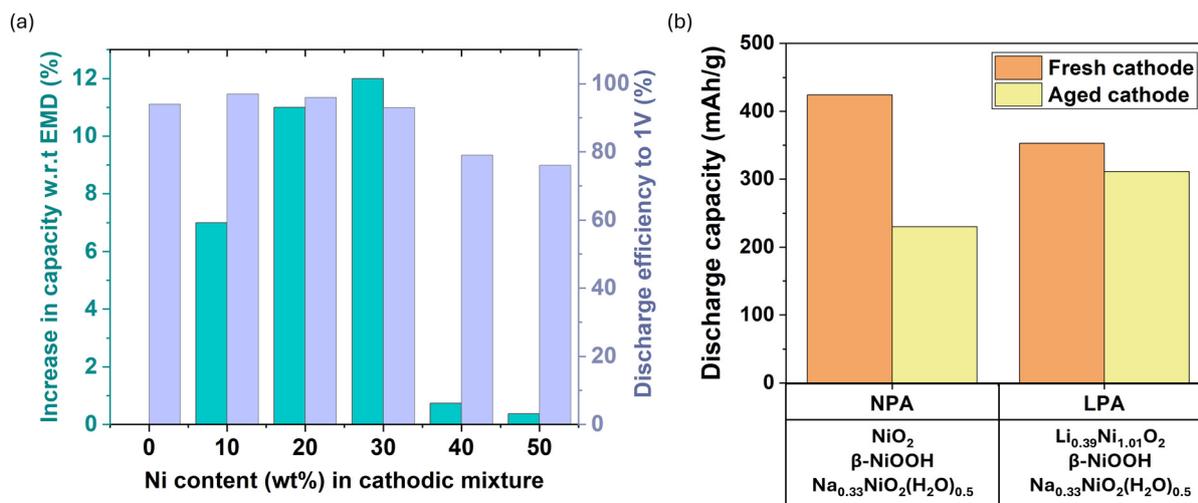
Fig. 11 (a) Percentage increase in discharge capacity with respect to EMD (green bars) and discharge efficiency at 1 V (blue bars) of the cathode mixtures of Ni oxide and EMD at different Ni contents (wt%).[111] (b) Comparison of the discharge capacities of two different multiphase Ni cathodes (NPA and LPA) before and after the aging test (24 h, room temperature).[111]

Table 2 Summary of cathode active material compositions prepared via design strategies under discussion in this review and their respective electrochemical performance data

Cathode active material composition	Design strategy adopted	Oxidation state of Ni	Fresh discharge capacity (mAh g⁻¹)	OCV (V)	Aging protocol	Discharge capacity after aging test (mAh g⁻¹)	Stability: Capacity retention after aging (%)	Ref.
EMD Tronox	NA	NA	287 (10 mA g⁻¹ to 0.8 V)	1.63	NA	NR	—	129
Li$_{0.3}$H$_{0.2}$NiO$_2$	Cation doping or substitution	+3.5	425 (10 mA g⁻¹ to 0.8 V)	1.95	NA	NR	—	129
Li$_{0.104}$NiO$_2$	Cation doping or substitution	+3.9	409 (10 mA g⁻¹ to 1.0 V)	1.8–2.0	Aging of cathode powders at 70 °C, 50% relative humidity for 4 weeks	157 (10 mA g⁻¹ to 1.0 V)	38	106
Na$_{0.33}$NiO$_2$(H$_2$O)$_{0.5}$	Cation doping or substitution	+3.67	347 (10 mA g⁻¹ to 1.0 V)	1.8–2.0		327 (10 mA g⁻¹ to 1.0 V)	94	106
8% Co-doped γ-NiOOH	Cation doping or substitution	+3.35	167 (C/20 discharge rate)	1.65–1.7	Store cell at 60 °C, 24 h prior to discharge	160 (C/20 discharge rate)	96	67
7% Fe-doped γ-NiOOH	Cation doping or substitution	+ 3.30	149 (C/20 discharge rate)	1.65–1.7		145–150 (C/20 discharge rate)	97	67
γ-NiOOH	NA	NR	123 (C/20 discharge rate)	1.6–1.65		31 (C/20 discharge rate)	25	67
Li$_{0.104}$NiO$_2$ with 0.33 wt% TiO$_2$ nano-coating on surface	Surface coating	+3.9	365 (10 mA g⁻¹ to 1.0 V)	1.9	Treat cathode powders with KOH electrolyte for 24 h at room temperature	270 (10 mA g⁻¹ to 1.0 V)	74	122
Multiphase cathode NPA	Multiphase cathode	+3.9	424 (10 mA g⁻¹ to 1.0 V)	1.9–1.95		230 (10 mA g⁻¹ to 1.0 V)	54	111
Multiphase cathode LPA	Multiphase cathode	+3.7	353 (10 mA g⁻¹ to 1.0 V)	1.9–1.95		311 (10 mA g⁻¹ to 1.0 V)	88	111
Mixture of LPA and EMD (weight ratio of Ni:Mn = 1)	Cathode composite	+3.9	292 (10 mA g⁻¹ to 1.0 V)	NR	Half-cell aging at 60 °C for 14 days	268 (10 mA g⁻¹ to 1.0 V)	92	111
Mixture of NPA and EMD (weight ratio of Ni:Mn = 1)	Cathode composite	+3.7	244 (10 mA g⁻¹ to 1.0 V)	NR	Half-cell aging at 60 °C for 14 days	214 (10 mA g⁻¹ to 1.0 V)	88	111
EMD Tronox	NA	NA	268 (10 mA g⁻¹ to 1.0 V)	NR	Half-cell aging at 60 °C for 14 days	257 (10 mA g⁻¹ to 1.0 V)	96	111
Nano NiOOH	Nanosizing	NR	282.2 (120 mA g⁻¹), 196.3 (10 000 mA g⁻¹)	1.85	NR	NR	—	85
Nano γ-NiOOH	Nanosizing	+3.65	350 (5 mA)	1.67–1.7	NR	NR	—	87
Nano NiOOH	Nanosizing	NR	250 (60 mA g⁻¹)	1.7	NR	NR	—	116

stability. Despite their excellent ability to refine the electro-chemical properties of nickel oxides, cation doping and surface coating approaches typically involve high-temperature solid-state or solution-based reactions, which require careful process optimisation to achieve desired improvement in cathode properties. Instead, multi-phase/composite cathodes combine the advantages of various electrochemically active materials. A key benefit of preparing cathode composites of high-valent nickel oxides and/or EMD is the reduction of the cathode fabrication costs by minimising the use of expensive nickel-based precursors while still increasing the overall discharge capacity and voltage of the cathode beyond that of conventional EMD. In addition, the incorporation of EMD and/or more chemically stable Ni oxide compounds in the cathode composite would improve the overall stability of the Ni-based cathode in alkaline electrolytes.

Recently, it was discovered that maintaining the content of Ni at approximately 20–30 wt% in the preparation of cathodic mixtures of high-valent nickel oxide and EMD resulted in a reasonable improvement in discharge capacity and discharge efficiency (where discharge efficiency is the ratio of the practical discharge capacity of a cathode mixture of nickelate and EMD at 1.0 V to the expected capacity based on individual material capacities) compared to the 100 wt% Mn cathode and the 50 wt% Ni-based cathode, as summarized in Fig. 11a.[111] Alternatively, mixtures or composites of various doped nickel oxide compounds in an optimal ratio could be utilised to achieve a nickel-based cathodic composition offering both high discharge capacity and lower aqueous reactivity in alkaline cells. For example, the employment of a mixture of nickel oxide phases, such as $Li_{0.39}Ni_{1.01}O_2$, $Na_{0.33}NiO_2(H_2O)_{0.5}$ and β-NiOOH, as a multiphase cathode composite referred to as LPA, resulted in a milder loss in discharge capacity and higher final capacity at the 1 V cutoff, compared to another nickel-based multiphase cathode comprising NiO_2, $Na_{0.33}NiO_2(H_2O)_{0.5}$ and β-NiOOH, referred to as NPA, even after 24 hours of powder aging in 40% KOH electrolyte (Fig. 11b).[111] This illustrates that the interlayer engineering of high-valent nickel oxides to incorporate structure stabilisers, such as Li and Na, is beneficial for simultaneously improving stability as well as maintaining decent discharge capacity in alkaline batteries.

Additionally, it was further discovered that a cathode mixture comprising 50 wt% Mn (EMD) + 50 wt% Ni (multi-phase Ni oxide, LPA) delivered a higher discharge capacity compared to commercial EMD, even after aging for 14 days at 60 °C, as recorded in Table 2.[111] This alludes to the improved chemical stability of such Ni–Mn hybrid cathodes, which exploit the higher chemical stability of MnO_2 to offset the greater interfacial reactivity of nickel oxides in alkaline media to generate a superior cathode for alkaline batteries. In essence, the discharge capacities and oxidation states of Ni in various well-known nickel oxide compounds provide the basis for optimising the ratio of different nickel oxides and/or MnO_2 in the advanced formulation of nickel-based cathode composites to achieve a superior electrochemical performance, com-pared to the traditional MnO_2 cathode, while maintaining decent chemical stability.

5. Performance benchmarking and comparative analysis

Various atomic-level and nanoscale engineering approaches for fabricating high-valent nickel-based cathodes for primary alkaline battery applications and their relevant nanoscale implications on the electrochemical performance have been discussed so far. This section aims to consolidate the cathode design strategies, chemical compositions and available discharge performance data for all the cathode active materials discussed in this review for evaluation against commercial EMD. Fig. 12 depicts a concise summary of the main takeaways from the present review regarding cathode engineering strategies for Ni cathodes in primary alkaline batteries and their relevant nanoscale phenomena under examination.

Cation doping or substitution involves tuning of NiO_2 layers in nickel oxide/hydroxide compounds or interlayer engineering to improve the bulk stability of the cathode in alkaline electrolyte by controlling the oxidation state of Ni and introducing charge-balancing species into the basic crystal structure. The molar quantities of Li, Na, K and H_2O in the final doped high-valent nickel oxide will influence the oxidation state of Ni, chemical stability and discharge capacity of the final cathode. To achieve divalent/trivalent metal substitution of Ni within NiOOH cathodes to stabilise the γ-NiOOH/α-Ni(OH)$_2$ couple, it is recommended to prepare α-Ni(OH)$_2$ substituted with a dopant of choice (e.g. Co^{2+}, Al^{3+}, and Fe^{2+}), followed by oxidation to a γ-NiOOH analogue. Nanosizing of high-valent nickel oxides boosts cathode kinetics via the reduction of the travel distances of protons to match the characteristic diffusion length suitable for cathode materials (based on the diffusion coefficient) and an increase in electrolyte penetration within the cathode for improving rate capability in alkaline batteries. Multifunctional surface coatings (e.g. CoOOH), which are ionically insulating yet electronically conducting, can be applied to protect the Ni^{4+}/Ni^{3+} rich inner core from electrolyte-induced self-discharge to enhance the overall cathode stability while increasing the discharge capacity relative to the bare MnO_2 cathode due to improved electronic conduction and cathode utilisation.

To extract key trends relating the chemical composition, the oxidation state of Ni and the electrochemical characteristics of all high-valent nickel cathodes evaluated for primary alkaline battery applications to date, Table 2 consolidates the cathode active material compositions of representative Ni cathodes achieved by various cathode engineering strategies (cation doping/substitution, nanosizing, surface coating and multiphase cathode/cathode composites), as well as their corresponding electrochemical performance data.

Generally, a higher oxidation state of Ni in the final cathode active material translates to a higher OCV and discharge
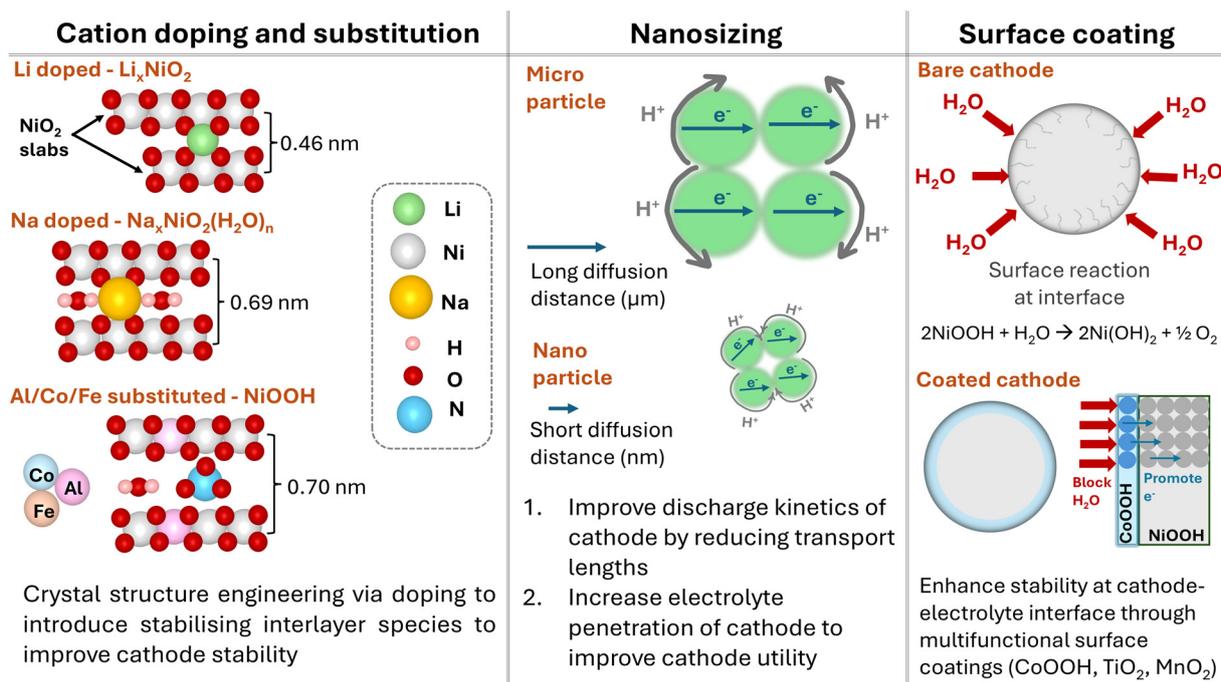
Fig. 12 Overview of the cathode design strategies and the accompanying nanoscale phenomena/features covered in this review.

capacity of a freshly assembled Ni cathode. This is evident from high-valent Ni cathodes prepared with 0.1 to 0.4% Li or Na dopant exhibiting a higher OCV of 1.8 to 1.9 V compared to the NiOOH cathodes (1.65 to 1.7 V), which correlates well with the improved oxidation state of Ni in the former (+3.5 and above) than in the latter (+3.3). However, a highly oxidised Ni cathode, such as $Li_{0.104}NiO_2$, also demonstrates poor cathode stability, quantified by the percentage retention of fresh discharge capacity after aging tests, owing to insufficient charge-balancing metal dopants, surface coating or multiphase composites incorporating structure stabilisers, as discussed in the previous section. There is a wide variation in aging or stability assessment protocols reported for different Ni cathodes in the literature: treatment of the cathode for 24 hours in an electrolyte prior to cell assembly, aging of the cathode in half-cell assembly at 60 °C for 14 days or 24 hours, and aging of the cathode powders at 70 °C and 50% relative humidity for 4 weeks. In addition, two studies that have explored the effects of Al substitution and CoOOH surface coating on the discharge performance of the NiOOH cathode have resorted to volume measurement of oxygen gas evolved during 16 days of storing cathode powder in 9 M KOH at 60 °C (Fig. 10) to evaluate the cathode stability. However, the nanosized NiOOH cathodes have not been subjected to stability tests to evaluate the effect of nanosizing on the chemical stability of high-valent nickel cathodes. Such a discrepancy in aging or stability tests makes it difficult to compare the stability levels of all high-valent Ni cathodes reported in different studies. Nevertheless, the exceptional improvement in the fresh capacity retention of TiO_2-coated $Li_{0.104}NiO_2$ (74%) relative to the bare $Li_{0.104}NiO_2$ (38%) after aging, while maintaining higher OCV and discharge

capacity compared to EMD, renders surface coating a promising nanoscale strategy for managing interfacial reactivity between the cathode and alkaline electrolyte, which merits further development.

Owing to its versatility in the accommodation of charge-compensating or structure-stabilising species, such as Al, Co, Fe, Na, K and/or H_2O, within its layered structure, γ-NiOOH can exist in a wide spectrum of chemical compositions, as examined in this review. The wide variation in the reported discharge capacities of various γ-NiOOH cathodes in Table 2 could be attributed to several factors, including the properties (morphology, microstructure, tap density, and specific surface area) of the Ni precursor used for the NiOOH synthesis, choice of Ni precursor (β-Ni(OH)$_2$, Ni(NO$_3$)$_2$, NiCl$_2$ or NaNiO$_2$), oxidisers (NaClO/K$_2$S$_2$O$_8$), nanostructural features, final oxidation of state of Ni, and actual chemical composition of the final cathode,[12,13,115] which have not been fully reported in some studies. This underscores the importance of comprehensive optimisation of the chosen synthesis route in the preparation of high-valent nickel cathodes, delivering the maximum possible discharge capacity while maintaining reasonable cathode stability for primary battery applications. For performance benchmarking of Ni cathodes against EMD, a plot of the fresh discharge capacity against stability (quantified by the percentage of fresh/initial discharge capacity retained after aging protocol) of all representative nickel-based cathodes, whose data are available, is presented in Fig. 13.

Out of all the high-valent nickel cathodes evaluated, the Ni cathodes prepared *via* alkali metal doping (Na$_{0.33}$NiO$_2$(H$_2$O)$_{0.5}$) and the multiphase cathode composites (LPA composite and mixture of EMD and LPA) demonstrate higher or comparable
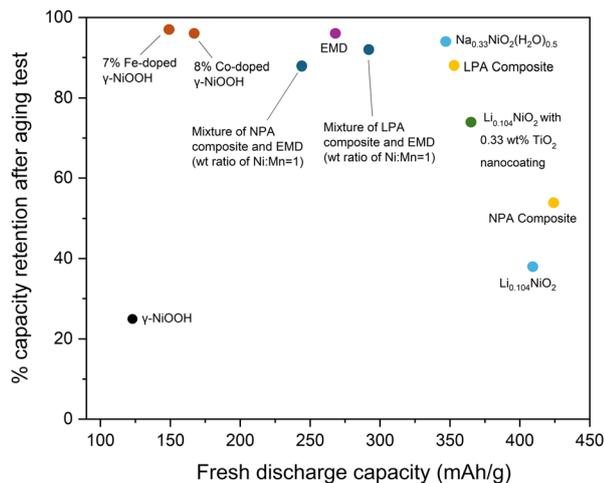
Fig. 13 Benchmarking of the discharge performances of representative-engineered Ni cathodes examined in this review against commercial EMD based on the fresh discharge capacity of the cathode (mAh g^{-1}) and percentage retention of the fresh cell capacity after the aging test (%).

fresh discharge capacity and stability, compared to the commercial EMD. This is attributed to the beneficial effect of partial doping of Li and Na, as well as the optional incorporation of interlayer H_2O, on cathode stability, while the maintenance of a sufficiently high Ni oxidation state (+3.5 to 3.7) in the metal-doped/substituted nickel oxides enables the achievement of high discharge capacities. Therefore, the quantity of metal doped or substituted is key for balancing the oxidation state of Ni, fresh discharge capacity and stability of the final Ni cathode. While single-phase highly delithiated $Li_{0.104}NiO_2$ exhibits a high Ni oxidation state, accompanied by low cathode stability, increasing the Li dopant concentration from 0.1 to 0.39 mole of Li per mole of Ni (as in $Li_{0.39}Ni_{1.01}O_2$, as part of the LPA composite) enables the sufficient stabilisation of the NiO_2 layers with Li^+ and the simultaneous lowering of the Ni oxidation state to improve the overall bulk cathode stability in alkaline media. Alternatively, employing an oxidiser, such as sodium persulfate, in the preparation of highly oxidised nickel cathodes, generates a partially sodium-doped single-phase $Na_{0.33}NiO_2(H_2O)_{0.5}$ incorporating Na and H_2O as structure stabilisers, which exhibits one of the highest fresh discharge capacities out of all cathode candidates while maintaining reasonably high OCV and stability comparable to that of EMD.

Despite their remarkably high stability in alkaline electrolytes, Fe and Co-substituted γ-NiOOH exhibit much lower fresh discharge capacities than EMD, making them less attractive compositions to pursue. Interestingly, the inappropriate particle morphology of NiOOH, which maintains optimal electronic contact with conductive carbon in the cathode, has been deemed responsible for the poor discharge performance of freshly assembled Fe and Co-substituted γ-NiOOH cathodes.[67] Therefore, it would be prudent to monitor the particle morphology in future optimisation studies of the synthesis of

high-valent nickel oxides to achieve reasonably high discharge capacities. For instance, Al-substituted γ-NiOOH, exhibiting a spherical morphology, high tap density (1.51 g cm^{-3}) and average Ni oxidation state of +3.57, delivered a high discharge capacity (353 mAh g^{-1} at 30 mA g^{-1} current density), as well as improved storage stability in a 9 M KOH solution.[115] Such a wide performance gap between different cation-substituted γ-NiOOH samples highlights the importance of synthesis optimisation to achieve critical cathode properties necessary to realise both exceptional discharge performance and stability.

Nanosized NiOOH can deliver high discharge capacity (282 mAh g^{-1}), which matches or exceeds that of conventional EMD (287 mAh g^{-1} at 10 mA g^{-1}) at higher current rates of 120 mA g^{-1}, resulting from the enhancement of the transport kinetics within the cathode nanoparticles due to the reduced diffusion distances of protons. However, it is difficult to comment on the influence of the nanosizing of NiOOH on stability owing to the absence of aging test data. Moreover, surface coatings have proven beneficial in improving the stability of cathodes in alkaline media, relative to their uncoated counterparts, by tuning the interfacial reactivity at the cathode–electrolyte boundary, as evidenced by the reduced oxygen evolution from the CoOOH-coated NiOOH cathodes *via* self-discharge in Fig. 10b. However, there is still room for improvement regarding the stability of nanostructured high-valent nickel cathodes since the discharge capacity of TiO_2-coated $Li_{0.104}NiO_2$ after aging is still lower than that of EMD, as depicted in Fig. 13. Therefore, it is strongly recommended that any future studies on bulk or surface nanostructuring of high-valent nickel oxides for primary alkaline battery application must include extensive stability testing to truly assess the influence of various nanostructuring techniques on the chemical stability and shelf life of high-valent Ni cathodes.

As an alternative to the surface coating strategy, the formation of multiphase cathodes by combining various high-valent nickel oxides with varying Ni oxidation states, discharge capacities and crystal structures can likewise provide improved structural stability, as well as discharge performance, compared to single-phase $Li_{0.104}NiO_2$ or γ-NiOOH individually. The addition of EMD to the multiphase cathode composite can further enhance the overall stability of the hybrid cathode with some acceptable compromise on its fresh discharge capacity.

Three key performance metrics are suggested to be prioritized in future investigations to facilitate meaningful comparison and the eventual commercialization of high-valent Ni-based cathodes developed within laboratory settings. Firstly, the storage stability of engineered Ni cathodes with respect to standard β-NiOOH and EMD (MnO_2) cathodes at room temperature and elevated temperatures (*e.g.* 60 °C) should be monitored by measurements of O_2 gassing volumes at different durations. This would provide an accurate measure of the shelf-life of the Ni cathode since O_2 generation is associated with the self-discharge reaction as discussed earlier. Secondly, the discharge capacity, voltage and specific energy density for newly developed Ni cathodes should be measured alongside β-NiOOH and EMD cathodes right after battery assembly and

after several days of storage at room temperatures and elevated temperatures. Thirdly, rate capability tests are required at low and high discharge rates used in actual household devices (*e.g.* digital cameras, flashlights, remote controls) to assess the suitability of Ni cathodes for high-drain and high-power applications as desired. In addition, electrochemical tests should be conducted with Ni cathodes in full-cell configurations (Ni/Zn primary button cell or AA cylindrical cell) beyond 3-electrode half cells to validate the superiority of the Ni–Zn battery performance in commercial battery configurations mimicking realistic discharge conditions as closely as possible. Such electrochemical performance data of Ni cathodes would complement the storage stability data to provide a quantitative assessment of the competitiveness of as-developed Ni cathodes in the primary alkaline battery market relative to the existing NiOOH and MnO_2 variants.

Based on a detailed analysis of various nanoscale engineered Ni cathodes reported in literature, the formation of an optimal single-phase Ni oxide structure capable of proton uptake, exhibiting a high Ni oxidation state and appropriate particle size and morphology, was found to be essential to outperforming EMD in terms of fresh discharge capacity and voltage. In that regard, highly oxidised nickel cathodes doped with 30% to 40% sodium and lithium, as well as NiOOH nanorods, were able to fulfil the above requirements and deliver superior fresh discharge capacity compared to EMD. The incorporation of structure stabilisers, such as Li, Na, Al, Fe, Co and/or H_2O, is necessary to enhance the bulk stability of single-phase high-valent Ni cathodes in alkaline electrolytes by nanoscale optimisation of NiO_2 slabs and the interslab region. Therefore, structural optimisation of single-phase nickel oxide sets the ceiling for the achievable outstanding discharge performance of the Ni cathode in primary alkaline batteries. Other cathode engineering strategies, such as nanosizing, surface coating and composite formation, serve as complementary measures to address electronic conductivity and electrode–electrolyte interface stability issues necessary for the practical discharge capacity of Ni cathode to approach the desired performance ceiling.

6. Challenges and outlook

The present review consolidates past and present advances achieved in the development of high-valent nickel oxide cathodes to unveil suitable cathode engineering strategies and nanoscale considerations for designing next-generation primary Ni–Zn alkaline batteries. Unlike previous reviews on nickel cathodes (mainly $Ni(OH)_2$ type), which have focused on improving the cycling stability and energy density of Ni cathodes for the rechargeable Ni–Zn battery, the present discourse has examined several cathode engineering strategies through a nanoscale lens for primary alkaline battery applications. The proposed cathode strategies targeted at achieving superior voltage and discharge capacity of high-valent nickel cathodes are cation doping/substitution, nanosizing, surface coating

and multiphase/composite cathodes. Beyond a mere compilation of existing literature on Ni cathodes evaluated for primary alkaline battery application, this review seeks to uncover critical nanoscale phenomena responsible for the electrochemical capacity and stability of high-valent nickel cathodes, namely the diffusion kinetics of protons/electrons, stabilisation of the layered structure of Ni oxide and cathode–electrolyte interfacial reactivity. This is accomplished by a detailed examination, comparative analysis and performance benchmarking of representative high-valent nickel cathodes reported in journal and patent literature, which serve to enlighten readers on the intricate relationship between cathode architecture, nanoscale phenomena and electrochemical performance.

Having established the nanoscale phenomena controlling the kinetics and stability of high-valent Ni cathodes in primary alkaline batteries, there are two remaining challenges that need to be tackled to realise the transition from manganese to nickel-based primary alkaline batteries in the future. The first challenge is the unresolved nanoscale origins of the chemical instability of high-valent Ni oxides. Although high-valent nickel oxides showcase attractive voltages and multi-electron redox capabilities, their practical application as the cathode in primary alkaline batteries is fundamentally limited by chemical instability, which originates from the nanoscale. As experimentally confirmed in previous works, pristine high-valent Ni oxides exhibit significant self-discharge and oxygen evolution when stored in concentrated alkaline electrolytes. Such instability is not only associated with the bulk material composition, but also is closely related to nanoscale surface chemistry, defect structures and thermodynamics of interfacial hydration of Ni cathodes in alkaline media. In spite of the proposed cation doping/substitution and surface coating measures to stabilise cathode crystal structure and cathode–electrolyte boundary, respectively, the identification and regulation of other nanoscale descriptors, such as surface defect density and local Ni oxidation state distribution, have yet to be performed.

Another challenge is the limited understanding of proton–electron diffusion pathways at the nanometer length scale, which directly influences the discharge capacity and rate capability of high-valent nickel oxide cathodes. Although nanosizing and nanostructuring approaches are widely employed to reduce the diffusion length and boost reaction kinetics, they are inevitably accompanied by undesired side reactions, due to the increased surface area of cathode particles in contact with the electrolyte. Therefore, it is necessary to optimise the cathode particle design to maximise the proton and electron conductivity while minimising parasitic reactions at the cathode–electrolyte interface. This will facilitate simultaneous improvements of the discharge capacity, rate capability and chemical stability.

The future development of high-valent nickel cathodes depends on establishing a quantitative relationship between structure, stability and nanoscale transmission, instead of the gradual optimisation of the cathode formulation. Beyond traditional bulk and surface characterisation techniques, such as

Scanning Electron Microscopy (SEM), XRD and Fourier Transform Infrared Spectroscopy (FTIR), it is advisable to conduct in-operando nanoscale characterisation studies during the storage, aging and electrochemical discharge of the cathode to monitor essential nanoscale descriptors, such as surface defects, distribution and evolution of Ni valence state and intercalated species within the crystal structure. For instance, operando X-ray Photoelectron Spectroscopy (XPS) is useful for capturing real-time valence state and chemical state data on surface species formed from parasitic reactions of Ni cathodes during the storage or battery operation.[130] Operando XRD and Electrochemical Quartz Crystal Microbalance (EQCM) are suitable techniques for elucidating proton transport mechanisms and surface hydration phenomena occurring within emerging or newly discovered Ni cathode compositions.[131] Given the high reactivity of Ni^{4+}/Ni^{3+} under ambient conditions, cryo-Transmission Electron Microscopy (cryo-TEM) may be employed to study the growth of crystal defects and nanostructures on the cathode surface while shielding the cathode–electrolyte interface from beam damage.[132] Such comprehensive nanoscale examination during discharge or storage of Ni cathodes would enrich the current understanding of nanoscale phenomena, limiting performance in primary alkaline batteries to guide future optimisation studies towards solving existing performance bottlenecks.

From an economic and industry standpoint, the high cost of nickel (US\$ 15.15 per kg)[133] compared to manganese (US\$ 1.18 per kg)[134] mandates the exploration of strategies to simplify and reduce the cost of fabricating nickel-based cathodes, since cost is a critical determinant of the commercialisation potential of a battery technology. Apart from employing hybrid cathode composites of EMD and high-valent nickel oxides, as discussed in section 4.4, to reduce costs and improve cathode stability, recycling of nickel-based primary batteries would be essential to ensure a circular economy for expensive nickel precursors and maintain battery costs within reasonable margins. Despite the projected elevated development costs of Ni–Zn primary batteries upon initial commercialisation, the anticipated performance gains for high-drain devices, such as power tools, wireless keyboards and electric clocks, justify the switch to Ni–Zn chemistry. Such niche, high-value applications are most likely to be the first use cases of this revolutionary technology.

Author contributions

Deepika Ranganathan: conceptualisation, visualisation, writing – original draft and writing – review and editing; Yi Cai: conceptualisation and writing – review and editing; Madhavi Srinivasan: supervision, funding acquisition and writing – review and editing.

Conflicts of interest

All the authors of this review article are listed as inventors in a joint patent application (18/301,544) filed between Nanyang Technological University and Energizer Holdings, Inc., which has been cited in this article.

Data availability

No primary research results, software or code have been included, and no new data were generated or analysed as part of this review.

Acknowledgements

References

1 Y. Liang, C.-Z. Zhao, H. Yuan, Y. Chen, W. Zhang, J.-Q. Huang, D. Yu, Y. Liu, M.-M. Titirici, Y.-L. Chueh, H. Yu and Q. Zhang, *InfoMat*, 2019, **1**, 6–32.

2 A. M. Vassallo, in *Advances in Batteries for Medium and Large-Scale Energy Storage*, ed. C. Menictas, M. Skyllas-Kazacos and T. M. Lim, Woodhead Publishing, 2015, pp. 587–607, DOI: 10.1016/B978-1-78242-013-2.00017-0.

3 S. Ponnada, M. S. Kiai, R. Krishnapriya, R. Singhal and R. K. Sharma, *Energy Fuels*, 2022, **36**, 6013–6026.

4 BU-106: Advantages of Primary Batteries, https://batteryuniversity.com/article/bu-106-advantages-of-primary-batteries, (accessed August 2025).

5 H. Rahimi-Eichi and M.-Y. Chow, in *The World Scientific Handbook of Energy*, World Scientific, 2012, vol. 3, pp. 405–426.

6 A. Gao, Z. Sun, S. Li, X. Hou, H. Li, Q. Wu and X. Xi, *Dalton Trans.*, 2018, **47**, 3864–3871.

7 D. Linden and B. McDonald, *J. Power Sources*, 1980, **5**, 35–55.

8 J. Thakur, P. Phogat, S. Sharma, R. Jha and S. Singh, *Phys. Chem. Chem. Phys.*, 2025, **27**, 4045–4077.

9 H. J. Bergveld, W. S. Kruijt and P. H. L. Notten, in *Battery Management Systems: Design by Modelling*, ed. H. J. Bergveld, W. S. Kruijt and P. H. L. Notten, Springer Netherlands, Dordrecht, 2002, pp. 31–53, DOI: 10.1007/978-94-017-0843-2_3.

10 M. Intelligence, Primary Battery Market Size & Share Analysis - Growth Trends & Forecasts (2025–2030), https://www.mordorintelligence.com/industry-reports/global-primary-battery-market-industry, (accessed 21 April 2025).

11 R. M. Dell, *Solid State Ionics*, 2000, **134**, 139–158.

12 X.-Z. Fu, Y.-J. Zhu, Q.-C. Xu, J. Li, J.-H. Pan, J.-Q. Xu, J.-D. Lin and D.-W. Liao, *Solid State Ionics*, 2007, **178**, 987–993.

13 E. Shangguan, H. Tang, Z. Chang, X.-Z. Yuan and H. Wang, *Int. J. Hydrogen Energy*, 2011, **36**, 10057–10064.

14 Y. Sun, J. Pan, P. Wan and X. Liu, *Mater. Res. Bull.*, 2009, **44**, 943–946.

15 M. T. Castro, J. A. D. del Rosario-Paraggua and J. D. Ocon, *Chem. Eng. Trans.*, 2022, **94**, 301–306.

16 Alkaline Battery Market Size and Forecast 2025 to 2034, https://www.precedenceresearch.com/alkaline-battery-market, (accessed August 2025).

17 G. Pistoia, in *Batteries for Portable Devices*, ed. G. Pistoia, Elsevier Science B.V., Amsterdam, 2005, pp. 33–76, DOI: 10.1016/B978-044451672-5/50004-1.

18 D. Qiu, B. Li, C. Zhao, J. Dang, G. Chen, H. Qiu and H. Miao, *Energy Storage Mater.*, 2023, **61**, 102903.

19 S. Le, L. Zhang, X. Song, S. He, Z. Yuan, F. Liu, N. Zhang, K. Sun and Y. Feng, *J. Electrochem. Soc.*, 2019, **166**, A2980.

20 K. Kordesh and M. Weissenbacher, *J. Power Sources*, 1994, **51**, 61–78.

21 M. B. Lim, T. N. Lambert and E. I. Ruiz, *J. Electrochem. Soc.*, 2020, **167**, 060508.

22 Y. Dai, J. Zhang, X. Yan, G. Zhao, M. Yang, J. Xiong, R. Li, N. Miao, H. Yu, M. Hu, J. Liu and J. Yang, *Chem. Eng. J.*, 2023, **471**, 144158.

23 B. J. Hertzberg, A. Huang, A. Hsieh, M. Chamoun, G. Davies, J. K. Seo, Z. Zhong, M. Croft, C. Erdonmez, Y. S. Meng and D. Steingart, *Chem. Mater.*, 2016, **28**, 4536–4545.

24 17.5: Batteries and Fuel Cells, https://chem.libretexts.org/Courses/University_of_Kentucky/UK%3A_General_Chemistry/17%3A_Electrochemistry/17.5%3A_Batteries_and_Fuel_Cells, (accessed August 2025).

25 J. F. Johansen, T. W. Farrell and C. P. Please, *J. Power Sources*, 2006, **156**, 645–654.

26 E. Moazzen, E. V. Timofeeva and C. U. Segre, *J. Mater. Sci.*, 2017, **52**, 8107–8118.

27 X. Liu, C. Chen, Y. Zhao and B. Jia, *J. Nanomater.*, 2013, **2013**, 736375.

28 X. Wang and Y. Li, *Chem. – Eur. J.*, 2003, **9**, 300–306.

29 S. Kanungo, K. Parida and B. Sant, *Electrochim. Acta*, 1981, **26**, 1147–1156.

30 S. Park, H.-W. Shim, C. W. Lee, H. J. Song, I. J. Park, J.-C. Kim, K. S. Hong and D.-W. Kim, *Nano Res.*, 2015, **8**, 990–1004.

31 C. Julien, M. Massot and C. Poinsignon, *Spectrochim. Acta, Part A*, 2004, **60**, 689–700.

32 M. Voinov, *Electrochim. Acta*, 1982, **27**, 833–835.

33 M. Manickam, P. Singh, T. B. Issa, S. Thurgate and R. De Marco, *J. Power Sources*, 2004, **130**, 254–259.

34 C. Mondoloni, M. Laborde, J. Rioux, E. Andoni and C. Lévy-Clément, *J. Electrochem. Soc.*, 1992, **139**, 954.

35 A. Biswal, B. C. Tripathy, K. Sanjay, T. Subbaiah and M. Minakshi, *RSC Adv.*, 2015, **5**, 58255–58283.

36 G. Blomgren and J. Hunter, in *Kirk–Othmer Encyclopedia of Chemical Technology*, 2000, https://doi-org.remotexs.ntu.edu.sg/10.1002/0471238961.1618091302121513.a01.

37 E. Faegh, T. Omasta, M. Hull, S. Ferrin, S. Shrestha, J. Lechman, D. Bolintineanu, M. Zuraw and W. E. Mustain, *J. Electrochem. Soc.*, 2018, **165**, A2528.

38 K. Kordesch, J. Gsellmann and K. Tomantschger, *J. Electroanal. Chem. Interfacial Electrochem.*, 1981, **118**, 187–201.

39 S. Chen, M. Zhang, P. Zou, B. Sun and S. Tao, *Energy Environ. Sci.*, 2022, **15**, 1805–1839.

40 H. Al-Salih and Y. Abu-Lebdeh, *J. Mol. Liq.*, 2025, **422**, 127179.

41 F. R. McLarnon and E. J. Cairns, *J. Electrochem. Soc.*, 1991, **138**, 645.

42 M. B. Lim, T. N. Lambert and B. R. Chalamala, *Mater. Sci. Eng., R*, 2021, **143**, 100593.

43 K. Bogomolov and Y. Ein-Eli, *ChemSusChem*, 2024, **17**, e202300940.

44 B. D. Desai, J. B. Fernandes and V. K. Dalal, *J. Power Sources*, 1985, **16**, 1–43.

45 R. J. Brodd, A. Kozawa and K. V. Kordesch, *J. Electrochem. Soc.*, 1978, **125**, 271C.

46 M. Beley and J. Brenet, *Electrochim. Acta*, 1973, **18**, 1003–1011.

47 A. Mondal and H. T. Das, in *Ceramic Science and Engineering*, ed. K. P. Misra and R. D. K. Misra, Elsevier, 2022, pp. 323–351, DOI: 10.1016/B978-0-323-89956-7.00008-5.

48 X. Jia, C. Liu, Z. G. Neale, J. Yang and G. Cao, *Chem. Rev.*, 2020, **120**, 7795–7866.

49 E. D. Spoerke, H. Passell, G. Cowles, T. N. Lambert, G. G. Yadav, J. Huang, S. Banerjee and B. Chalamala, *MRS Energy Sustainability*, 2022, **9**, 13–18.

50 K. Kordesch and J. Daniel-Ivad, *Handbook of Batteries*, McGraw-Hill, New York, 2002.

51 J. B. Fernandes, B. D. Desai and V. K. Dalal, *J. Power Sources*, 1985, **15**, 209–237.

52 M. P. Chavhan, S. R. Sethi and S. Ganguly, *J. Energy Storage*, 2020, **32**, 101851.

53 M. Huang, F. Li, F. Dong, Y. X. Zhang and L. L. Zhang, *J. Mater. Chem. A*, 2015, **3**, 21380–21423.

54 W. Wei, X. Cui, W. Chen and D. G. Ivey, *Chem. Soc. Rev.*, 2011, **40**, 1697–1721.

55 X.-P. Gao and H.-X. Yang, *Energy Environ. Sci.*, 2010, **3**, 174–189.

56 M. B. Kumbhar, V. V. Patil, V. S. Chandak, J. L. Gunjakar and P. M. Kulal, *J. Alloys Compd.*, 2025, **1010**, 177311.

57 M. B. Kumbhar, V. V. Patil, V. S. Chandak, S. B. Shaikh, Y. M. Chitare, J. L. Gunjakar and P. M. Kulal, *J. Ind. Eng. Chem.*, 2025, **147**, 422–435.

58 M. B. Kumbhar, V. V. Patil, V. S. Chandak, Y. M. Chitare, J. L. Gunjakar and P. M. Kulal, *J. Solid State Electrochem.*, 2025, **29**, 2687–2705.

59 P. Oliva, J. Leonardi, J. Laurent, C. Delmas, J. Braconnier, M. Figlarz, F. Fievet and A. De Guibert, *J. Power Sources*, 1982, **8**, 229–255.

60 H. Bode, K. Dehmelt and J. Witte, *Electrochim. Acta*, 1966, **11**, 1079–1087.

61 D. S. Hall, D. J. Lockwood, C. Bock and B. R. MacDougall, *Proc. R. Soc. A*, 2015, **471**, 20140792.

62 M. Casas-Cabanas, J. Canales-Vázquez, J. Rodríguez-Carvajal and M. R. Palacín, *Mater. Res. Soc. Symp. Proc.*, 2009, **1126**, 131–136.

63 M. Casas-Cabanas, M. D. Radin, J. Kim, C. P. Grey, A. Van der Ven and M. R. Palacín, *J. Mater. Chem. A*, 2018, **6**, 19256–19265.

64 C.-C. Yang, *Int. J. Hydrogen Energy*, 2002, **27**, 1071–1081.

65 B. Liu, X. Liu, X. Fan, J. Ding, W. Hu and C. Zhong, *J. Alloys Compd.*, 2020, **834**, 155185.

66 L. Zhang, R. Qin, Y. Pan, Z. Duan, Y. Li, N. Xi, L. Jian and S. Han, *Int. J. Hydrogen Energy*, 2022, **47**, 1083–1091.

67 F. Bardé, M. R. Palacin, B. Beaudoin, P. Christian and J.-M. Tarascon, *J. Power Sources*, 2006, **160**, 733–743.

68 R. Huggins, H. Prinz, M. Wohlfahrt-Mehrens, L. Jörissen and W. Witschel, *Solid State Ionics*, 1994, **70**, 417–424.

69 X. Yang, K. Takada, M. Itose, Y. Ebina, R. Ma, K. Fukuda and T. Sasaki, *Chem. Mater.*, 2008, **20**, 479–485.

70 H. Arai, M. Tsuda, M. Hayashi, H. Ohtsuka and Y. Sakurai, *Electrochim. Acta*, 2005, **50**, 1821–1828.

71 L. F. Huang, M. J. Hutchison, R. J. Santucci, Jr., J. R. Scully and J. M. Rondinelli, *J. Phys. Chem. C*, 2017, **121**, 9782–9789.

72 Y. Sun, N. Liu, J. Pan and P. Wan, *Int. J. Electrochem. Sci.*, 2018, **13**, 2718–2730.

73 J. Pan, Y. Sun, P. Wan, Z. Wang and X. Liu, *Electrochem. Commun.*, 2005, **7**, 857–862.

74 E. S. Davydova, Y. Halpern, A. Breytus and A. Rothschild, *Solid State Ionics*, 2025, **422**, 116815.

75 A. Van der Ven, D. Morgan, Y. S. Meng and G. Ceder, *J. Electrochem. Soc.*, 2006, **153**, A210.

76 Y. Elbaz, D. Furman and M. C. Toroker, *Phys. Chem. Chem. Phys.*, 2018, **20**, 25169–25178.

77 G. Feuillade and R. Jacoud, *Electrochim. Acta*, 1969, **14**, 1297–1311.

78 O. Guiader and P. Bernard, *J. Electrochem. Soc.*, 2018, **165**, A396.

79 J. Gallenberger, H. M. Fernández, A. Alkemper, M. Li, C. Tian, B. Kaiser and J. P. Hofmann, *Catal. Sci. Technol.*, 2023, **13**, 4693–4700.

80 B. E. Conway and P. L. Bourgault, *Can. J. Chem.*, 1959, **37**, 292–307.

81 P. L. Bourgault and B. E. Conway, *Can. J. Chem.*, 1960, **38**, 1557–1575.

82 B. E. Conway and P. L. Bourgault, *Can. J. Chem.*, 1962, **40**, 1690–1707.

83 B. E. Conway and P. L. Bourgault, *Trans. Faraday Soc.*, 1962, **58**, 593–607.

84 O. Diaz-Morales, D. Ferrus-Suspedra and M. T. M. Koper, *Chem. Sci.*, 2016, **7**, 2639–2645.

85 J. Pan, Y. Sun, Z. Wang, P. Wan, Y. Yang and M. Fan, *J. Power Sources*, 2009, **188**, 308–312.

86 X.-Z. Fu, Q.-C. Xu, R.-Z. Hu, B.-X. Pan, J.-D. Lin and D.-W. Liao, *J. Power Sources*, 2007, **164**, 916–920.

87 L. Liu, Z. Zhou and C. Peng, *Electrochim. Acta*, 2008, **54**, 434–441.

88 J. Chen, D. H. Bradhurst, S. X. Dou and H. K. Liu, *J. Electrochem. Soc.*, 1999, **146**, 3606.

89 S. Natarajan, M. Ulaganathan and V. Aravindan, *J. Mater. Chem. A*, 2021, **9**, 15542–15585.

90 Y. Morioka, S. Narukawa and T. Itou, *J. Power Sources*, 2001, **100**, 107–116.

91 P. Bernard and M. Lippert, in *Electrochemical Energy Storage for Renewable Sources and Grid Balancing*, ed. P. T. Moseley and J. Garche, Elsevier, Amsterdam, 2015, pp. 223–251, DOI: 10.1016/B978-0-444-62616-5.00014-0.

92 ZAF's Nickel Zinc Prismatic, https://zafsys.com/nizn-batteries/nizn-prismatic/.

93 BC2: UPS Battery Cabinet, https://zincfive.com/products/bc-series-ups-battery-cabinets/?tab=1.

94 H. Luo, B. Liu, Z. Yang, Y. Wan and C. Zhong, *Electrochem. Energy Rev.*, 2022, **5**, 187–210.

95 Z. Zhao, X. Fan, J. Ding, W. Hu, C. Zhong and J. Lu, *ACS Energy Lett.*, 2019, **4**, 2259–2270.

96 J. Deng, X. Sun and H. Peng, *EcoMat*, 2023, **5**, e12343.

97 A. M. Crespi, S. K. Somdahl, C. L. Schmidt and P. M. Skarstad, *J. Power Sources*, 2001, **96**, 33–38.

98 F. Bardé, M. Palacin, B. Beaudoin and J.-M. Tarascon, *Chem. Mater.*, 2005, **17**, 470–476.

99 H. Arai and Y. Sakurai, *MRS Online Proc. Libr.*, 1999, **575**, 3.

100 H. Arai and Y. Sakurai, *J. Power Sources*, 1999, **81**, 401–405.

101 H. Arai, M. Tsuda, K. Saito, M. Hayashi, K. Takei and Y. Sakurai, *J. Solid State Chem.*, 2002, **163**, 340–349.

102 M. Casas-Cabanas, J. Rodríguez-Carvajal, J. Canales-Vázquez and M. R. Palacín, *J. Mater. Chem.*, 2006, **16**, 2925–2939.

103 K. Mukai, J. Sugiyama and Y. Aoki, *J. Solid State Chem.*, 2010, **183**, 1726–1732.

104 T. Matsumura, R. Kanno, R. Gover, Y. Kawamoto, T. Kamiyama and B. J. Mitchell, *Solid State Ionics*, 2002, **152**, 303–309.

105 M. Casas-Cabanas, J. Canales-Vázquez, J. Rodríguez-Carvajal and M. R. Palacín, *Mater. Res. Symp. Proc.*, 2009, **1126**, 131–136.

106 G. Zheng, S. Dukuslow and D. Kelly, *US Pat*, 20240128449A1, 2024.

107 P. Kalyani and N. Kalaiselvi, *Sci. Technol. Adv. Mater.*, 2005, **6**, 689.

108 M. Bianchini, M. Roca-Ayats, P. Hartmann, T. Brezesinski and J. Janek, *Angew. Chem., Int. Ed.*, 2019, **58**, 10434–10458.

109 M. Lewis, B. Gaulin, L. Filion, C. Kallin, A. Berlinsky, H. Dabkowska, Y. Qiu and J. Copley, *Phys. Rev. B:Condens. Matter Mater. Phys.*, 2005, **72**, 014408.

110 P. Vassilaras, X. Ma, X. Li and G. Ceder, *J. Electrochem. Soc.*, 2012, **160**, A207.

111 D. Ranganathan, V. Siong, Y. Cai, M. Srinivasan and G. Zheng, *US Pat*, 20230361293A1, 2023.

112 C. Delmas, J. J. Braconnier, Y. Borthomieu and P. Hagenmuller, *Mater. Res. Bull.*, 1987, **22**, 741–751.

113 C. Delmas, J. J. Braconnier, Y. Borthomieu and M. Figlarz, *Solid State Ionics*, 1988, **28–30**, 1132–1137.

114 C. Faure, C. Delmas, M. Fouassier and P. Willmann, *J. Power Sources*, 1991, **35**, 249–261.

115 X.-Z. Fu, X. Wang, Q.-C. Xu, J. Li, J.-Q. Xu, J.-D. Lin and D.-W. Liao, *Electrochim. Acta*, 2007, **52**, 2109–2115.

116 J. Pan, J. Du, Y. Sun, P. Wan, X. Liu and Y. Yang, *Electrochim. Acta*, 2009, **54**, 3812–3818.

117 R. Jain, A. S. Lakhnot, K. Bhimani, S. Sharma, V. Mahajani, R. A. Panchal, M. Kamble, F. Han, C. Wang and N. Koratkar, *Nat. Rev. Mater.*, 2022, **7**, 736–746.

118 M. Bhar, U. Bhattacharjee, S. Ghosh and S. K. Martha, in *Nanostructured Materials Engineering and Characterization for Battery Applications*, ed. A. B. Gueye, H. J. Maria, N. Kalarikkal, M. Fall, A. M. Stephan and S. Thomas, Elsevier, 2024, pp. 575–600, DOI: 10.1016/B978-0-323-91304-1.00015-0.

119 G. W. D. Briggs and P. R. Snodin, *Electrochim. Acta*, 1982, **27**, 565–572.

120 C. Jiang, E. Hosono and H. Zhou, *Nano Today*, 2006, **1**, 28–33.

121 S.-K. Jung, I. Hwang, D. Chang, K.-Y. Park, S. J. Kim, W. M. Seong, D. Eum, J. Park, B. Kim, J. Kim, J. H. Heo and K. Kang, *Chem. Rev.*, 2020, **120**, 6684–6737.

122 G. Zheng and W. Huang, *US Pat*, 11611072B2, 2023.

123 P. K. Alaboina, M.-J. Uddin and S.-J. Cho, *Nanoscale*, 2017, **9**, 15736–15752.

124 J. Liang, J. Hu, T. Zhou, Y. Li, X. Ren, S. Huang, X. Yang, Q. Zhang and J. Liu, *Compos. Commun.*, 2022, **36**, 101356.

125 Q. Fan, K. Lin, S. Yang, S. Guan, J. Chen, S. Feng, J. Liu, L. Liu, J. Li and Z. Shi, *J. Power Sources*, 2020, **477**, 228745.

126 D. Uzun, M. Doğrusöz, M. Mazman, E. Biçer, E. Avci, T. Şener, T. C. Kaypmaz and R. Demir-Cakan, *Solid State Ionics*, 2013, **249–250**, 171–176.

127 Q. D. Wu, X. P. Gao, G. R. Li, G. L. Pan, T. Y. Yan and H. Y. Zhu, *J. Phys. Chem. C*, 2007, **111**, 17082–17087.

128 P. Benson, G. W. D. Briggs and W. F. K. Wynne-Jones, *Electrochim. Acta*, 1964, **9**, 275–280.

129 P. A. Christian, Y. Wang, N. K. Iltchev, K. S. Nanjundaswamy, J. A. Nelson and F. Zhang, *US Pat*, 11811058B2, 2023.

130 D.-J. Yun, S. Kim, S. Heo, H.-s. Choi, J. Baik, J. Chung, S. Park, D. Yu, J. Lee, S. Kang, C. Jung and D.-S. Ko, *Adv. Energy Mater.*, 2024, **14**, 2401473.

131 H. Guo, D. Goonetilleke, N. Sharma, W. Ren, Z. Su, A. Rawal and C. Zhao, *Cell Rep. Phys. Sci.*, 2020, **1**, 100225.

132 Y. Li, Y. Li, A. Pei, K. Yan, Y. Sun, C.-L. Wu, L.-M. Joubert, R. Chin, A. L. Koh, Y. Yu, J. Perrino, B. Butz, S. Chu and Y. Cui, *Science*, 2017, **358**, 506–510.

133 LME Nickel, https://www.lme.com/en/metals/non-ferrous/lme-nickel#Summary, (accessed August 2025).

134 Manganese Price Trend, Index and Forecast, https://www.imarcgroup.com/manganese-pricing-report, (accessed August 2025).